Tests of Compatibility Between Quantum Mechanics and Macroscopic Local Realism

Piotr Deuar

Project Supervisor: Dr. M. D. Reid

An IVH Project conducted at the Department of Physics
at the University of Queensland

11 November, 1996

Abstract

Quantum mechanical predictions for two states are checked for compatibility with hidden-variable theories dealing only with macroscopic "elements of reality" via the Bell inequalities. The states are: 1) A pair of spin-correlated high-spin particles or a pair of multiphoton states with correlated polarisation. 2) A particular quantum mechanical superposition of pairs of phase-correlated, spatially-separated coherent states whose properties are measured using a homodyne detection scheme. Both states are found to be incompatible with hidden-variable theories dealing with microscopic "elements of reality", but the second state is also found to be incompatible with macroscopic hidden-variable theories for appropriate values of its parameters. Here a macroscopic quantity is considered to be one whose physical value is undetermined to within an error which is itself macroscopic.

Contents

Introduction

Realism is a premise associated with the philosophical view that there exists a reality with definite properties irrespective of whether they are observed by someone or not. This is an underlying principle of classical physics, and many people have tried to devise interpretations of quantum mechanics that are manifestly consistent with realism (so-called hidden variable theories).

Another approach was taken by Einstein, Podolsky and Rosen[1][1]. Their argument is given in more detail in section 1.2. EPR gave a reasonable definition of realism, assumed this and no action-at-a-distance (locality), and showed that *with these premises*, the results of some measurements on a correlated system of particles are predetermined. This is not given by any quantum mechanical description of the system, so EPR concluded that the quantum mechanical description was incomplete. This is the so-called EPR paradox. Experimental results that confirm the paradox have recently been produced by Ou et al[2].

It was shown by Bell[3] in 1965, that *any* theory satisfying the above premises of locality and realism (local realism) gives results at odds with the predictions of quantum mechanics. Many experiments have been carried out since[4][5][6][7][8] to test this and the results of these generally vindicate quantum mechanics and reject local realism.

So far all the discrepancies that have been shown between quantum mechanics and local realism have pertained to microscopic measurements, and all experiments performed have been on microscopic systems (Here we define a macroscopic measurement as a measurement that has an uncertainty in measured value that is itself macroscopic[9]). The failure of local realism in microscopic

---

[1]referred to as EPR from now on.

systems or for microscopic measurements is perhaps not so surprising, as classical physics, which is intimately connected with realism, stops giving accurate predictions in the truly microscopic regime. The question whether quantum mechanics in the macroscopic limit should satisfy local realism (i.e. macroscopic local realism) is more contentious. One could argue that quantum mechanics should reduce to classical mechanics in the macroscopic limit, thus satisfying macroscopic local realism, but one could also point out that there seems to be nothing in quantum mechanics that forbids the formation of quantum superpositions of macroscopically distinct states[2] ,and these would not satisfy macroscopic local realism.

The aim of this project is to look at the quantum-mechanical predictions for some states, and check their compatibility with macroscopic local realism as the macroscopic limit is approached.

To this end, chapter 1 covers some basic concepts needed for an understanding of the methods and notation used to test the quantum mechanical predictions against macroscopic local realism. This includes definitions of local realism and macroscopic measurements, the Bell inequality that will be used, and how this may be extended to test for compatibility with *macroscopic* local realism[9]. The EPR argument is also covered in more detail.

Chapter 2 concerns itsef with a system that can be interpreted as two subsystems contsisting of photon modes that are correlated in polarisation, or two spin-correlated particles, having spin higher than $\frac{1}{2}$. (A version of the EPR paradox was given by Bohm[13] for this system, but with spin $\frac{1}{2}$). This system is found to be compatible with macroscopic, but not microscopic, local realism. Appendix A details some additional calculations used in the analysis of this state.

Chapter 3 looks at a system consisting of a superposition of pairs of phase-correlated coherent states that has been shown[14] to be able to be created by a non-degenerate parametric oscillator under certain ideal conditions. When quadrature phase measurements are performed on the system, the quantum mechanical predictions are found to be incompatible with *macroscopic* local realism for some parameter values. Appendix B details some additional calculations and proofs used in this analysis.

---

[2]so-called "Schrödinger-cat" states[10][11][12].

Chapter 1

Basic Concepts

1.1 Local Realism and Elements of Reality

The concepts of *local realism* and *element of reality* were first introduced by Einstein, Podolsky and Rosen in their 1935 paper on the EPR paradox[1].

Locality implies that a measurement performed, or event occurring in region A cannot instantaneously influence events or measurements in another region B, spatially separated from A, and conversely events and measurements in B cannot instantaneously influence events or measurements in A. Thus a measurement made in A has no effect on the result of a measurement being simultaneously performed in B and vice versa.

Realism states that if one can predict with certainity the result of a measurement on a system, without in any way disturbing that system, then the result of that measurement is a predetermined property of the system. EPR called these predetermined properties *elements of reality*.

Thus logically *Local Realism* is a combination of the above, i.e. no action-at-a-distance (Locality), and Realism.

Figure 1.1: Spatially separated particles correlated in position and momentum. Here x_n and p_n represent position and momentum of the nth particle
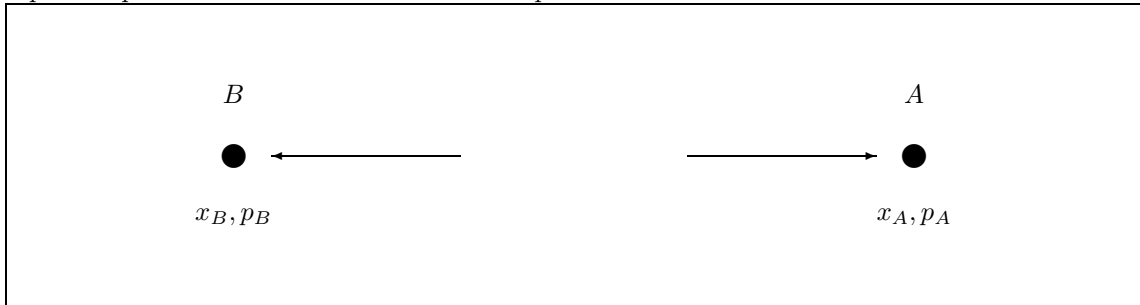
1.2 The EPR Paradox

The famous Einstein-Podolsky-Rosen argument is instructive in understanding the concepts of local realism, and its compatibility with quantum mechanics, which are central to this paper. The EPR argument has been formulated in various ways, perhaps the best known formulations are those of Bohm[13], and the original[1]. Here we will consider the original formulation.

The EPR argument was originally given as an attempt to show that the quantum mechanical description of a system is incomplete. Three premises, which seemed reasonable at the time, were given:

1. *Locality*: There is no action-at-a-disatance in nature.

2. *Realism*: "If without in any way disturbing a system, we can predict with certainty (i.e., with probability equal to unity) the value of a physical quantity, then there exists an element of physical reality corresponding to this physical quantity"[1].

3. Some of the quantum-mechanical predictions about the results of measurements on the system under consideration[1] are correct.

The system under consideration consists of two particles, spatially separated, but correlated in position and momentum (Figure 1.1). Systems like this are known to be predicted by quantum mechanics. As the systems (call them A and B) are perfectly correlated, one can infer the result

---

[1]see immediately below.

of a simultaneous position measurement at B, by measuring the position of A, (and conversely infer the result of a position measurement on A by measuring the position of B). Similarily if one performs a momentum measurement on A at time t, one can infer the result of a momentum measurement at B at this same time t. Now beacuse locality has been postulated, a measurement of position (say) at A at time t cannot disturb the particle at B until possibly at some later time, so we can predict the result of a measurement of the position of the particle B at time t without disturbing that system. These are the conditions required to be able to say that assuming realism, there exists an element of reality corresponding to the position of particle B at time t. Let us call this element of reality $x_B(t)$. By an equivalent chain of reasoning we can infer the existence of other elements of reality for the system, such as $x_A(t)$ (position of particle A at t) and $p_A(t)$, $p_B(t)$ (the momenta of particles A and B at t).

Now by the realism assumption, $x_A(t)$ and the other elements of reality, are predetermined properties of the system, that have an existence irrespective of whether the measurement whose result we can infer is carried out or not.

Now the crux of the EPR argument is that we have inferred that for a particle (say A), both position x_A and momentum p_A have definite predetermined values, something that cannot be given by any quantum mechanical description of the system, since quantum mechanics cannot give accuracy beyond that given by the Heisenberg uncertainty relationship $\Delta x \Delta p \geq \hbar/2$. EPR thus then concluded that, at least for this system, the quantum-mechanical description of the system must be incomplete.

Paraphrasing the above statements, we could theoretically contrive some apparatus to measure the position or momentum (not both simultaneously, of course), of one of these particles to a sufficient accuracy, such that the following situation occurs: We measure the position of particle A at time t to an accuracy Δx_A, and simultaneously measure the momentum of particle B to an accuracy Δp_B. But we can now infer the value of the momentum of particle A at t because of the correlation of the particles. For simplicity lets assume the correlation implies $p_A = -p_B$, say.

Then the momentum of particle A at time t is known to an accuracy $\Delta p_A = \Delta p_B$, and we can, assuming local realism, theoretically make measuring devices that will give $\Delta p_A \Delta x_A < \hbar/2$.[2]

So by adopting the seemingly reasonable postulates of locality and realism, we are led to conclude that quantum mechanics is incomplete. Perhaps a more lucid formulation of this is:

either: locality and realism hold, but quantum mechanics cannot be complete

or: locality or realism are false (or both), and quantum mechanics may be complete.

EPR hoped that a more complete theory would perhaps be of the "hidden variable" variety.

1.3   Tests of Local Realism: Bell's Theorem

EPR had apparently supposed that the assumptions of local realism were compatible with quantum mechanics. However work by Bell, and others[3][15], starting in 1965, essentially proved this assumption false. The original version of Bell's theorem[3] was based on Bohm's version of the EPR argument[13], pertaining to a system containing two spatially separated spin-$\frac{1}{2}$ particles, whose spins are correlated. Bell showed that the assumptions of locality and existence of elements of reality constrained the results of measurements on the system to obey an inequality. (One of the so called "Bell inequalities"). The results of certain such measurements are predicted by quantum mechanics to violate this inequality. Thus quantum mechanics is incompatible with the assumption of local reality.

A quick overview of the proof of Bell's theorem by Clauser and Horne[16] follows, as this result will be used in subsequent sections. A more detailed analysis of this and other Bell inequalities may be found in a paper by Clauser and Shimony[15]. This proof was originally formulated for spin-$\frac{1}{2}$ particles going through polarisers, but the proof is more general and can be applied to any pair of spatially separated systems for which measurements involving an adjustable parameter give binary outcomes. Consider a pair of spatially separated but mutually correlated systems, A and B

---

[2] This last statement can cause confusion, and it should be noted that there is no claim here that the Heisenberg uncertainty principle is wrong, as the Δ's here do *not* represent measurements of position and momentum on a single particle, only the inferred values of their corresponding elements of reality. The actual measurements outlined above are performed on two separate particles, and do not violate the HUP.

(Figure 1.2). The systems, (e.g. spin-$\frac{1}{2}$ particles) pass through "analysers" on the way to their detectors. The analyser properties depend on parameter(s)[3] a and b which are under the control of the experimenter.

Now suppose that for one or more values of the analyser parameters, we have perfect correlation between the systems A and B. We can now follow the argument of section 1.2 through, and by assuming local realism, deduce the existence of elements of reality corresponding to the values of the measurements A_a and B_b. As quantum mechanics does not predict the results of single measurements, the fact that we can supposedly do so here suggests that there is a more complete specification of the system which can predict these results. Such a description would be a so-called "hidden variable" theory[4]. This description is commonly denoted λ[5].

Let us now suppose that the detectors can give only one of two outcomes for a measurement: *count / no-count*, or *yes / no*, etc. Denote the probability of obtaining a result of *count* at detector A, given analyser parameters a to be P_A, and the probability of obtaining a result of *count* at detector B, given analyser parameter b to be P_B. Also define the joint probability of obtaining a *count* at both detectors to be P_{AB}. Now from the locality assumption we can say that P_A will be independent of the parameter b, and correspondingly P_B will be independent of a, as the systems, as well as the detectors and analysers are spatially separated. Thus the probabilities will depend only on the overall state λ and their local analyser parameters. We have: $P_A(\lambda, a)$, $P_B(\lambda, b)$, $P_{AB}(\lambda, a, b)$ as the probabilities for a given a,b, and λ. Furthermore, locality states that we can write

$$P_{AB}(\lambda, a, b) = P_A(\lambda, a)P_B(\lambda, b) \tag{1.1}$$

Now Clauser and Horne introduce the lemma, which is proved in their paper[16]

If x,x',y,y',X,Y are real numbers such that $0 \leq x,x' \leq X$ and $0 \leq y,y' \leq Y$ then,

---

[3] a and b may represent a whole set of numbers

[4] A "deterministic hidden variable theory" is defined to be any physical theory which predicts or postulates the existence of states in which the observables of quantum mechanics have definite values, as opposed to just giving probabilities of obtaining certain values upon measurement as in quantum mechanics itself.

[5] Here λ may represent a whole set of parameters for describing the state, not necessarily just one number.

Figure 1.2: Two quantum-correlated systems at spatially separated locations A and B. a and b are analyser parameters, A_a and B_b are values measured by the detectors.
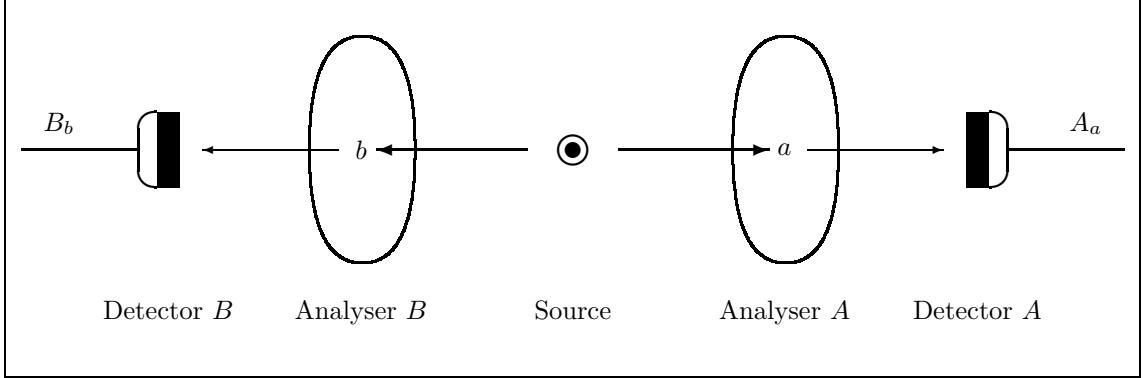
$$-XY \quad \leq \quad xy - xy' + x'y + x'y' - Yx' - Xy \quad \leq \quad 0 \tag{1.2}$$

Now (1.1) and (1.2) give.

$$-1 \leq P_{AB}(\lambda, a, b) - P_{AB}(\lambda, a, b') + P_{AB}(\lambda, a', b) + P_{AB}(\lambda, a', b') - P_A(\lambda, a') - P_B(\lambda, b) \leq 0 \tag{1.3}$$

If we have an ensemble of these correlated two-part systems, and the probability of any one of these systems of having a hidden variable description of λ is $\rho(\lambda)$, then we have the ensemble average probabilities

$$
\begin{aligned}
P_A(a) &= \int P_A(\lambda, a) d\rho(\lambda) \\
P_B(b) &= \int P_B(\lambda, b) d\rho(\lambda) \\
P_{AB}(a, b) &= \int P_{AB}(\lambda, a, b) d\rho(\lambda)
\end{aligned}
\tag{1.4}
$$

These ensemble average probabilities are now the properties of the system that correspond to probabilities calculated via quantum mechanics. So by taking the ensemble average of the right side of (1.3) and manipulating, we get the final version of the Bell inequality that we'll be using in further parts of this paper:

$$\frac{P_{AB}(a, b) + P_{AB}(a', b) + P_{AB}(a', b') - P_{AB}(a, b')}{P_A(a') + P_B(b)} \leq 1 \tag{1.5}$$

This inequality must be satisfied by any local hidden variable theory, irrespective of the details of such a theory, and if any violations of this inequality are found experimentally, all local hidden variable theories must be rejected. (See section 1.4 below for more on this)

There is a whole family of inequalities, of which (1.5) is one member, which go collectively under the name of Bell inequalities, and must be satisfied by systems to be compatible with hidden variable theories. They are essentially equivalent, with some more general than others, and more suited to paticular experimental or theoretical systems and configurations. Equation (1.5) is the most convenient to use in this paper. Clauser and Shimony[15] give many of the best known versions.

1.4 Experimental Evidence

So far, the the correlated particles considered in the original EPR argument[1] (section 1.2) have not been demonstrated to exist, but a version of the EPR paradox which is essentially equivalent[17], but using quadrature phase measurements of photon fields instead of position and momentum measurements of particles, has been achieved in an experiment by Ou et al[2]. Where before it could have been argued that the EPR paradox was only an idealised case which cannot be in fact produced experimentally, this experiment has shown the paradox to be experimentally realisable, giving new weight to the question of whether quantum mechanics is compatible with local realism[18].

Over the last twenty or so years, various experiments have been carried out to test for violations of the Bell inequalities. There are difficulties in performing an experimental test of these inequalities, as they assume perfect correlation, 'analyser properties', and detector efficiencies. This is unrealistic for real experiments. To get around the problem, some auxilliary assumptions have to be used, but if these are well chosen, they can be expected to hold for all but some pathological systems[15].

Aspect et al and others[4][5][6][7][8] have also succeeded in demonstrating a violation of Bell inequalities, supported by some auxilliary assumptions which have been mentioned before. Thus it is almost inevitable that local realism must be rejected.

1.5   Microscopic and Macroscopic Local Realism

Based on various versions of Bell's theorem and experiments that have been carried out (see section 1.4), it must be concluded that local realism is an untenable premise. It will however be argued later in this thesis that local realism may be rejected on a macroscopic, not just microscopic scale. The following discussion follows along the line of the article by Reid and Deuar[9].

Let us first define what we mean by a 'macroscopic' experiment. Define a *macroscopic* experiment to be one in which the uncertainty or error in the measured quantities is itself macroscopic. In the alternate case, where uncertainty in measurement is microscopic, we have a 'microscopic' experiment. Thus we would consider a measurement of position to an accuracy of say ± 1nm to be microscopic, while a measurement with error ± 1cm to be macroscopic. Similarily if we were measuring a component of angular momentum (say), which can only be measured to have discrete values (with separation $\hbar$), to an accuracy of $\pm \hbar$, this would be a microscopic measurement.

A measurement is often said to be 'macroscopic' if the system upon which it is performed contains a large number of particles, or has large spatial dimensions. Upon closer inspection, this definition of macroscopic seems to be erroneous. For example, one would not consider a detailed measurement of the position of a paticular atom in a crystal (say to within 1Å) as macroscopic, simply because the crystal had macroscopic dimensions, or contained a large number of particles. The definition of macroscopic used here is different, and excludes such cases as the example above.

What do we mean by 'macroscopic local realism'? Let us consider an experiment in which only macroscopic measurements are performed. Now in a similar way to section 1.1, we define:

Macroscopic Locality implies that a macroscopic measurement performed in region A cannot instantaneously influence any macroscopic measurements made in another region B, spatially separated from A. And conversely, any macroscopic measurements made in region B cannot instantaneously influence the results of macroscopic measurements in region A.

This definition says nothing about any microscopic changes which a measurement at A may instantaneously cause to the results of measurements at B, but since these are microscopic, they

do not affect the macroscopic measurements. For example in the original formulation of the EPR experiment (figure 1.1), if position was being measured to an accuracy of ± 1mm, at both A and B (i.e. we are measuring x_A and x_B), and we have macroscopic locality, then a measurement of x_A could not instantly affect the measurement of x_B by 2mm, however it could easily affect it by 1μm, as this small microscopic change would be swamped out by the size of the measurement uncertainty, making no difference to the resulting macroscopic measurement. Thus it can be seen that:

$$\text{microscopic locality}^6 \Rightarrow \text{macroscopic locality}$$

$$\text{macroscopic locality} \nRightarrow \text{microscopic locality}$$

(1.6)

Macroscopic Realism implies that if one can predict with certainty the result of a macroscopic measurement on a system, without physically disturbing that system, then the result of that macroscopic measurement is a predetermined property of the system: a macroscopic "element of reality". Macroscopic elements of reality have an associated indeterminacy associated with them, e.g. position $= 1\pm0.001$m.

Obviously *Macroscopic Local realism* is a combination of the above, i.e. Macroscopic Locality and Macroscopic Realism.

1.6   Implications of Macroscopic Local Realism

The failure of microscopic local realism, which we are led to conclude by Bell's theorem coupled with recent experimental evidence, is perhaps not so surprising, given that the microscopic realm is the realm of all sorts of thoroughly non-classical quantum phenomena, and hidden-variable theories are largely 'classical' in nature. In the macroscopic realm, however, it would be remarkable if local realism failed. Since macroscopic local realism rules out the possibility of superpositions of macroscopically distinct states, its failure would be as remarkable as the creation of 'Schrödinger-cat' states[10][11][12][19][20][21].

The EPR argument (section 1.2) is still valid and its conclusions still apply if we restrict

---

[6] usually referred to as just 'locality'

ourselves to considering only the postulate of *macroscopic* local realism and *macroscopic* elements of reality[9]. Thus for some systems, the assumption of macroscopic local realism is sufficient to imply the incompleteness of quantum mechanics[18]. This has been pointed out by Reid[18] to be a consequence of the results of the experiment performed by Ou et al[2]. This forces on us the choice of whether macroscopic local realism or the completeness of quantum mechanics must be rejected, and gives strong motivation for further investigation.

1.7   Bell Inequality Tests for Macroscopic Local Realism

Given the discussion above (section 1.6), we would like a way to determine whether the quantum mechanical predictions for a system violate macroscopic local reality, thus giving an avenue for experimental tests of macroscopic local realism vs. quantum mechanics.

One can use the Bell inequality (1.5) to test for compatibility of measurements with local realism on a microscopic level. Suppose we are measuring the quantum mechanical operator $\hat{A}$ on system A, spatially separated, but correlated with system B, where we measure the operator $\hat{B}$. We can define the result of a measurement $\mathcal{A}$ of $\hat{A}$ to be labelled '*count*' if $\mathcal{A}$ is measured in some range $\mathcal{R}_{\mathcal{A}}$, and '*no-count*' otherwise. Similarily we define '*count*' and '*no-count*' for measurements $\mathcal{B}$ of $\hat{B}$ at B using range $\mathcal{R}_{\mathcal{B}}$. Thus using the formalism of section 1.3, the probability of *count* at A, P_A equals $P_{\mathcal{R}_{\mathcal{A}}}$, the probability that $\mathcal{A} \in \mathcal{R}_{\mathcal{A}}$, so $P_B = P_{\mathcal{R}_{\mathcal{B}}}$ is the probability that $\mathcal{B} \in \mathcal{R}_{\mathcal{B}}$, and $P_{AB} = P_{\mathcal{R}}$ is the probability that $\mathcal{A} \otimes \mathcal{B} \in \mathcal{R} = \mathcal{R}_{\mathcal{A}} \otimes \mathcal{R}_{\mathcal{B}}$. Note that $\mathcal{R}$ can be any arbitrary range, possibly disjoint.

Here, the ranges $\mathcal{R}$ are well defined, and microscopic measurements must be performed to differentiate a result of *count* and *no-count*, at least near the boundaries of the range, hence only microscopic local realism is tested. A method for determining whether quantum mechanical predictions for a system are compatible with macroscopic local realism has been pointed out by Reid[9]. Basically, simulated "noise" is added to the predicted measurements. The elements of reality with which hidden variable theories are concerned, can be deduced from measurements

done on the system, so if the magnitude of this simulated "noise" is increased sufficiently to cause macroscopic uncertainties in the values of the elements of reality, and the Bell inequality is still violated, then one must conclude that the violation is due to the failure of macroscopic local realism, as all the microscopic predictions have been swamped by the noise.

Thus, by adding simulated noise to the quantum mechanical predictions of a system and entering the probabilities of obtaining these noisy measurements into the Bell inequalities, the compatibility of quantum mechanics with macroscopic local realism can be investigated.

The remainder of this paper concerns itself with two quantum mechanical systems: the so called 'higher spin' states and a superposition of coherent states, and determining whether quantum predictions for these systems are compatible with macroscopic local realism.

Chapter 2

Higher Spin States

The higher spin states defined in this chapter are the most obvious macroscopic[1] generalisation of the correlated spin-$\frac{1}{2}$ particle state considered originally in Bohm's *gedanken experiment*[13]. and Bell's theorem[3]. We consider correlated spin-s particles instead, where s$\rightarrow \infty$. These higher spin states, first tested for compatibility with local realism by Mermin[22], have already been shown to violate microscopic local realism[22][23][24][25][26][27][28][29][30][31][32], and thus seem to be good candidates for a possible violation of macroscopic local realism.

To test for macroscopic violations of the Bell inequality, I started with small simulated noise in the measurements, and increased the magnitude of the noise until the Bell inequality was no longer violated. If this noise term could be increased to significant values, with the violation still occurring, then the quantum mechanical predictions for this system could be said to be incompatible with macroscopic local realism. This was not the case.

---

[1]Here macroscopic refers to "large number of particles", not anything to do with accuracy of measurement, which we haven't considered yet.

2.1   The Higher Spin States

The higher spin state that is being considered is:

$$|\psi\rangle = \frac{1}{N!\sqrt{N+1}} \left[\hat{a}_+^\dagger \hat{b}_+^\dagger + \hat{a}_-^\dagger \hat{b}_-^\dagger \right]^N |0\rangle_A |0\rangle_B \tag{2.1}$$

Here $\hat{a}_\pm^\dagger$ are boson creation operators for a pair of fields in region A, spatially separated from another region B which has another pair of fields whose creation operators are $\hat{b}_\pm^\dagger$. $|0\rangle_A$ and $|0\rangle_B$ are vacuum states in regions A and B. In Bohm's EPR argument and Bell's original theorem, N was taken to be equal to 1. Here, higher values of N will be considered.

The state that is being considered here is actually given in terms of boson states, thus there may be some confusion as to why it has been called a "spin state". We can define the operators

$$
\begin{aligned}
\hat{S}_x^A &= \tfrac{1}{2} \left[\hat{a}_+^\dagger \hat{a}_- + \hat{a}_-^\dagger \hat{a}_+ \right] & \hat{S}_x^B &= \tfrac{1}{2} \left[\hat{b}_+^\dagger \hat{b}_- + \hat{b}_-^\dagger \hat{b}_+ \right] \\
\hat{S}_y^A &= \tfrac{1}{2i} \left[\hat{a}_+^\dagger \hat{a}_- - \hat{a}_-^\dagger \hat{a}_+ \right] & \hat{S}_y^B &= \tfrac{1}{2i} \left[\hat{b}_+^\dagger \hat{b}_- - \hat{b}_-^\dagger \hat{b}_+ \right] \\
\hat{S}_z^A &= \tfrac{1}{2} \left[\hat{a}_+^\dagger \hat{a}_+ - \hat{a}_-^\dagger \hat{a}_- \right] & \hat{S}_z^B &= \tfrac{1}{2} \left[\hat{b}_+^\dagger \hat{b}_+ - \hat{b}_-^\dagger \hat{b}_- \right]
\end{aligned}
\tag{2.2}
$$

These operators can easily be shown, using $\left[\hat{a}, \hat{a}^\dagger\right] = 1$ etc. to obey the commutation relations

$$
\begin{aligned}
\left[\hat{S}_x^A, \hat{S}_y^A\right] &= i\hat{S}_z^A & \left[\hat{S}_x^B, \hat{S}_y^B\right] &= i\hat{S}_z^B \\
\left[\hat{S}_y^A, \hat{S}_z^A\right] &= i\hat{S}_x^A & \left[\hat{S}_y^B, \hat{S}_z^B\right] &= i\hat{S}_x^B \\
\left[\hat{S}_z^A, \hat{S}_x^A\right] &= i\hat{S}_y^A & \left[\hat{S}_z^B, \hat{S}_x^B\right] &= i\hat{S}_y^B
\end{aligned}
\tag{2.3}
$$

Thus it can be recognized that the $\hat{S}$ operators are spin operators in the Schwinger formulation[33], and the state (2.1) can represent a pair of correlated spin $\frac{N}{2}$ particles as well as a system of bosons.

The fields $\hat{a}_\pm, \hat{b}_\pm$ can be transformed to give $\hat{c}_\pm$ and $\hat{d}_\pm$ fields by the transformation

$$
\begin{aligned}
\hat{c}_+ &= \hat{a}_+ \cos\theta + \hat{a}_- \sin\theta & \hat{c}_- &= \hat{a}_- \cos\theta - \hat{a}_+ \sin\theta \\
\hat{d}_+ &= \hat{b}_+ \cos\phi + \hat{b}_- \sin\phi & \hat{d}_- &= \hat{b}_- \cos\phi - \hat{b}_+ \sin\phi
\end{aligned}
\tag{2.4}
$$

Physically this corresponds to (for example) $\hat{a}_\pm$ being orthogonally polarised modes along some axes x, y, and $\hat{c}_\pm$ being orthogonally polarised modes along a different set of axes x', y' at an angle of θ to the original x, y. The transformation to $\hat{c}_\pm$ corresponds to the use of a polariser.

Figure 2.1: The Higher Spin experiment. Spatially separated, correlated bosonic modes $\hat{a}_\pm$ and $\hat{b}_\pm$ are created at the source, pass through polarisers with parameters θ and ϕ, and are separated into modes $\hat{c}_\pm$ and $\hat{d}_\pm$. The $\hat{c}_+$ and $\hat{d}_+$ modes are detected.
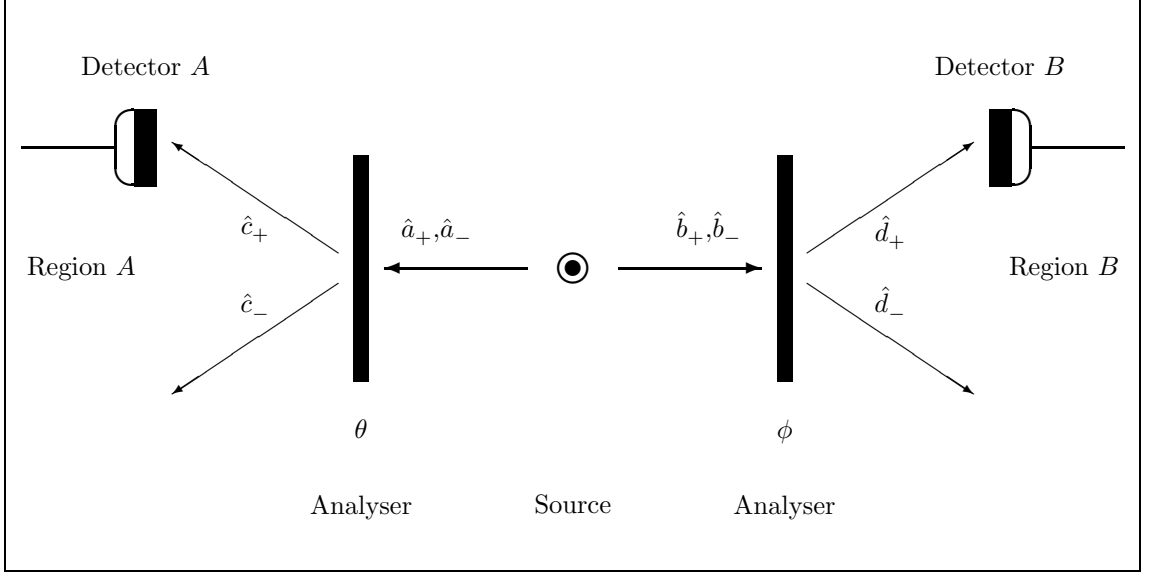
This situation is shown in figure 2.1. Alternatively this transformation can be interpreted as the measurement of spin components, in directions given by the angles θ, ϕ, for particles in the A, B regions respectively. The inverse transformation from the $\hat{c}, \hat{d}$ to the $\hat{a}, \hat{b}$ fields is

$$\hat{a}_+ = \hat{c}_+ \cos\theta - \hat{c}_- \sin\theta \qquad\qquad \hat{a}_- = \hat{c}_- \cos\theta + \hat{c}_+ \sin\theta$$
$$\hat{b}_+ = \hat{d}_+ \cos\phi - \hat{d}_- \sin\phi \qquad\qquad \hat{b}_- = \hat{d}_- \cos\phi + \hat{d}_+ \sin\phi \tag{2.5}$$

so we can rewrite the state as

$$|\psi\rangle = \frac{\left[\left(\hat{c}_+^\dagger \hat{d}_+^\dagger + \hat{d}_-^\dagger \hat{c}_-^\dagger\right)\cos(\theta - \phi) + \left(\hat{c}_+^\dagger \hat{d}_-^\dagger - \hat{c}_-^\dagger \hat{d}_+^\dagger\right)\sin(\theta - \phi)\right]^N}{N!\sqrt{N+1}} |0\rangle_{c_+} |0\rangle_{c_-} |0\rangle_{d_+} |0\rangle_{d_-} \tag{2.6}$$

Thus when $\theta = \phi$, the state is

$$|\psi\rangle = \frac{1}{N!\sqrt{N+1}} \left[\hat{c}_+^\dagger \hat{d}_+^\dagger + \hat{c}_-^\dagger \hat{d}_-^\dagger\right]^N |0\rangle_A |0\rangle_B \tag{2.7}$$

and the fields $\hat{c}_+$ & $\hat{d}_+$ and $\hat{c}_-$ & $\hat{d}_-$ are perfectly correlated, giving an EPR-like situation.

Note also that because the transformation (2.4) conserves boson number, and from the form of (2.1), the results of measurements on $\hat{c}_+^\dagger \hat{c}_+$ and $\hat{c}_-^\dagger \hat{c}_-$ will sum to N and similarly for $\hat{d}_+^\dagger \hat{d}_+$ and $\hat{d}_-^\dagger \hat{d}_-$.

2.2   Probability Distributions for the Higher Spin States

The measurements that are made on the system are measurements of photon number at the detectors, measuring $\hat{c}_+^\dagger \hat{c}_+$ and $\hat{d}_+^\dagger \hat{d}_+$. To evaluate the Bell inequality, one needs the probabilities of measuring various boson numbers at the detectors. The probability of measuring n bosons at detector A and m bosons at detector B, given the analyser parameters θ and ϕ, is

$$P_{nm}(\theta,\phi) = \left| \langle n|_{c_+} \langle N-n|_{c_-} \langle m|_{d_+} \langle N-m|_{d_-} |\psi\rangle \right|^2 = \Psi_{nm}^*(\theta,\phi)\Psi_{nm}(\theta,\phi) \qquad (2.8)$$

where we have also defined $\Psi_{nm}(\theta,\phi)$.

It can be shown[2] that

$$\Psi_{nm}(\theta,\phi) = \frac{\sqrt{n!m!(N-n)!(N-m)!}}{N!\sqrt{N+1}} \sum_{i=|n+m-N|\,\mathrm{div}\,2}^{(N-|n-m|)\,\mathrm{div}\,2} \begin{cases} \mathcal{K}_{N\theta\phi}(n,m,i) & \text{if } (n+m+N) \text{ is even} \\ \mathcal{K}_{N\theta\phi}\left(n,m,i+\tfrac{1}{2}\right) & \text{if } (n+m+N) \text{ is odd} \end{cases}$$
$$(2.9)$$

where the coefficients $\mathcal{K}$ are

$$\mathcal{K}_{N\theta\phi}(n,m,i) =$$
$$\binom{N}{2i} [\cos(\theta-\phi)]^{2i} [\sin(\theta-\phi)]^{N-2i} \binom{2i}{\tfrac{1}{2}(n+m-N)+i} \binom{N-2i}{\tfrac{1}{2}(n-m+N)-i} (-1)^{\frac{1}{2}(m-n+N)-i}$$
$$(2.10)$$

and the function div is defined as

$$x \,\mathrm{div}\, 2 = \begin{cases} \frac{x}{2} & \text{if x is even} \\ \frac{x}{2}-1 & \text{if x is odd} \end{cases} \qquad (2.11)$$

and n,m can take on any integer values $0,1,\ldots,N$. Note that the probability $P_{nm}(\theta,\phi)$ only depends of the difference $\theta-\phi$, not the actual values of these parameters by themselves. So one can write $\chi = \theta-\phi$ and

$$P_{nm}(\theta,\phi) = P_{nm}(\chi) \qquad (2.12)$$

The form of these probability distributions can be seen in figures 2.2. Additionally, $P_{nm}(\chi)$ has

---

[2]see Appendix A.1

Figure 2.2: Probability distributions for the higher spin state. Here the probabilities of measuring n photons at detector A and m photons at correlated detector B $(P_{nm}(\chi))$, for various experimental parameters χ, are displayed. All figures are for $N = 20$, except for figure 2.2f which has $N = 40$. Dark shading indicates high probability. Note that the magnitude of the probability P_{nm} represented by a given shading, varies between plots, as the sum total of P_{nm} must add to unity.

Figure 2.2a: $N = 20$, $\chi = 0$

Figure 2.2b: $N = 20$, $\chi = \pi/8$

Figure 2.2f: $N = 20$, $\chi = \pi/4$

Figure 2.2c: $N = 40$, $\chi = \pi/4$

Figure 2.2e: $N = 20$, $\chi = \pi/2$

Figure 2.2d: $N = 20$, $\chi = 3\pi/8$
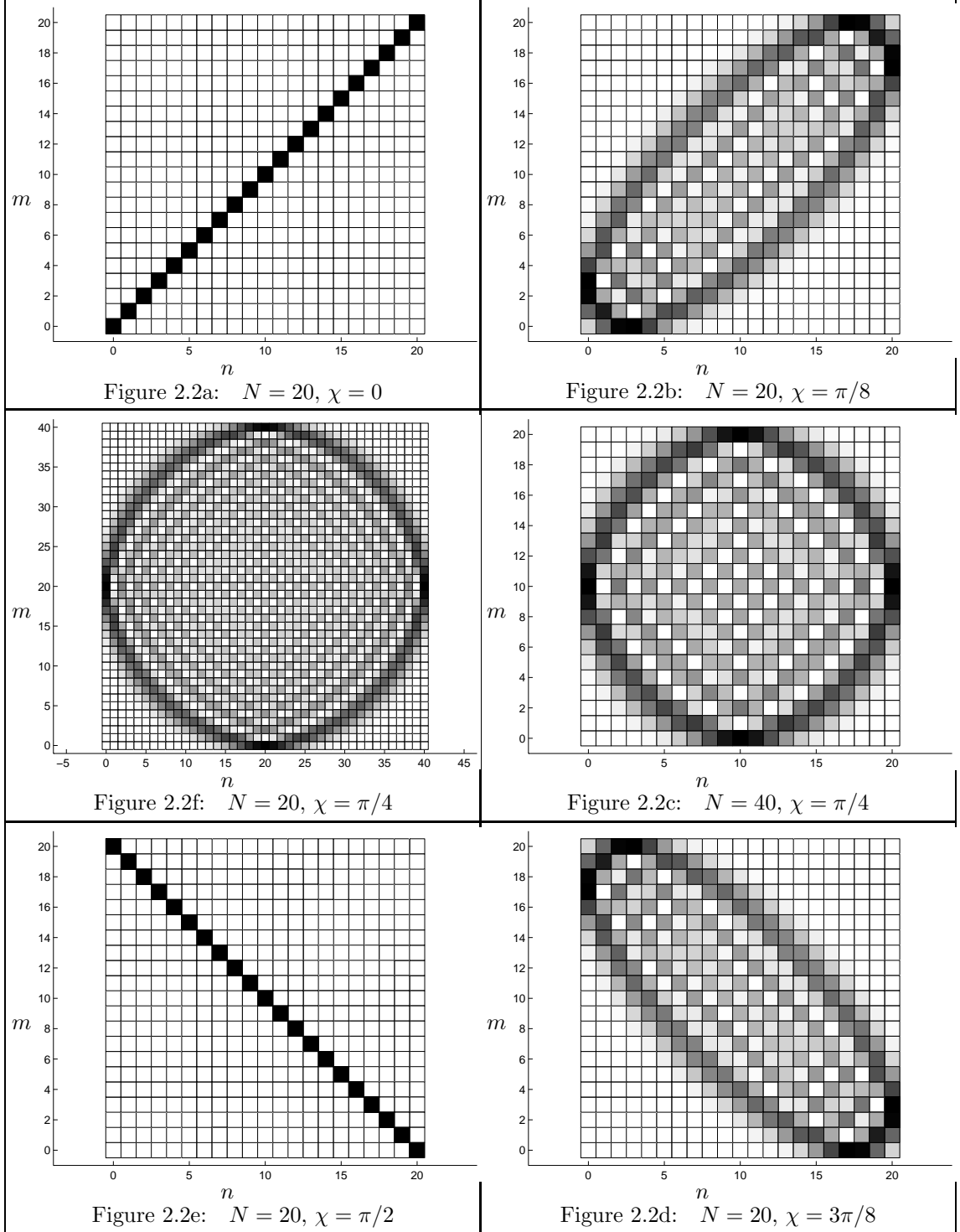
the properties[3]:

$$P_{nm}(\chi + \pi) = P_{nm}(\chi)$$

$$P_{nm}(\pi - \chi) = P_{nm}(\chi)$$

$$\therefore \qquad P_{nm}(\frac{\pi}{2} + \chi) = P_{nm}(\frac{\pi}{2} - \chi)$$

$$\& \qquad P_{nm}(\chi) = P_{nm}(|\chi|) \qquad (2.13)$$

$$P_{N-n,N-m}(\chi) = P_{nm}(\chi)$$

$$P_{mn}(\chi) = P_{nm}(\chi)$$

$$P_{N-n,m}(\chi - \frac{\pi}{2}) = P_{nm}(\chi)$$

some of which can be seen in figures 2.2.

The marginal probabilities $P_n(\theta)$, $P_m(\phi)$ giving the probability of measuring n , m bosons at detector A , B given analyser parameters θ , ϕ, respectively, are now given by:

$$P_n(\theta) = \sum_{m=0}^{N} P_{nm}(\chi) \qquad\qquad P_m(\phi) = \sum_{n=0}^{N} P_{nm}(\chi) \qquad (2.14)$$

If we define the ranges $\mathcal{R}_A$, $\mathcal{R}_B$ and $\mathcal{R}$ using the notation of section 1.7, then the probability of obtaining a measurment of *count* is given by

$$P_{\mathcal{R}}(\chi) = \sum_{(n,m) \in \mathcal{R}} P_{nm}(\chi) \qquad (2.15)$$

and the marginal probabilities are given by

$$P_{\mathcal{R}_A}(\theta) = \sum_{m \in \mathcal{R}_A} P_{nm}(\chi) \qquad\qquad P_{\mathcal{R}_B}(\phi) = \sum_{n \in \mathcal{R}_A} P_{nm}(\chi) \qquad (2.16)$$

2.3   Adding Noise

Now we wish to introduce simulated noise into the final measurement process. Let the noise be defined by the function $\varrho(\Delta_n, \Delta_m)$. Thus if the results of noiseless measurements at detectors A and B were (n, m) then the probability that the noisy measurement will give results in the range $(n + \Delta_n$ to $n + dn + \Delta_n$, $m + \Delta_m$ to $m + dm + \Delta_m)$ is given by $\varrho(\Delta_n, \Delta_m) \, dn \, dm$.

---

[3]See Appendix A.2

Note that now we are allowing the measurments of n and m to become continuous (in the range $-\infty$ to ∞). Thus we denote the results of noisy measurements by x and y, for measurements at the A and B detectors respectively. Let us now denote the probability of the noisy measurements being in the range (x to $x + dx$, y to $y + dy$) as $Q_{xy}(\chi)dx\,dy$. This is given by

$$Q_{xy}(\chi)\,dx\,dy = \sum_{nm} P_{nm}(\chi)\varrho(x - n, y - m)\,dx\,dy \qquad (2.17)$$

We still regard a measurement of *count* to occur if the (x, y) result lies in the range $\mathcal{R}$, but now $\mathcal{R}$ is continuous. The probability of measuring *count* is now

$$Q_{\mathcal{R}}(\chi) = \iint\limits_{(x,y)\in\mathcal{R}} Q_{xy}(\chi)\,dx\,dy \qquad (2.18)$$

Thus it can be seen that

$$Q_{\mathcal{R}}(\chi) = \sum_{n,m=0}^{N} P_{nm}(\chi)C_{nm}(\mathcal{R}) \qquad \text{where} \qquad C_{nm}(\mathcal{R}) = \iint\limits_{(x,y)\in\mathcal{R}} \varrho(x - n, y - m)\,dx\,dy \qquad (2.19)$$

Now we will assume independent noise sources at A and B, so that $\varrho(\Delta_n, \Delta_m)$ can be written as $\rho(\Delta_n)\rho(\Delta_m)$ in which case it is easier to use the "noise coefficients"

$$C_{nm}(\mathcal{R}) = C_n(\mathcal{R}_\mathcal{A})C_m(\mathcal{R}_\mathcal{B})$$

$$C_n(\mathcal{R}_\mathcal{A}) = \int\limits_{x\in\mathcal{R}_\mathcal{A}} \rho(x - n)\,dx \qquad (2.20)$$

2.4 Violations of the Bell Inequality for the Higher Spin States

The aim here is to search for violations of the Bell inequality by the higher spin states, as the measurements get more and more macroscopic. At first glance it seems reasonable that as the parameter N = "Number of particles" increases, the amount of noise that can be added to the measurements, while still violating the Bell inequality[4] also increases, thereby making the state violate macroscopic local realism at hign N.

---

[4]It is already known that the states will violate the Bell inequality with no noise for all N.
[22][23][24][25][26][27][28][29][30][31][32]

To this end the following questions were investigated:

1. For what values of the parameters $\theta, \phi, \theta', \phi'$ is the left hand side of the Bell inequality (1.5) maximised, giving maximum violation? (Subsection 2.4.1)

2. We must define the range of values $\mathcal{R}$ which will correspond to a result of *count*. What range $\mathcal{R}$ gives the largest violations of the Bell inequality? (Subsection 2.4.2)

3. How large can we make the noise before the Bell inequality is no longer violated for a given N? (Subsection 2.4.4)

4. Does the form of the noise (gaussian, box, etc.) have any significant impact on the answer to question 3? (Subsection 2.4.3)

5. Can the quantum mechanical predictions for the higher spin state be said to violate macroscopic local realism? (Section 2.5)

The probabilities to be substituted into the Bell inequality (1.5) are the noisy measurements $Q_\mathcal{R}$ and marginal probabilities $Q_{\mathcal{R}_A}, Q_{\mathcal{R}_B}$, thus we have:

$$B_\mathcal{R}(\theta, \chi, \theta', \chi') = \frac{Q_\mathcal{R}(\theta, \phi) + Q_\mathcal{R}(\theta', \phi) + Q_\mathcal{R}(\theta', \phi') - Q_\mathcal{R}(\theta, \phi')}{Q_{\mathcal{R}_A}(\theta') + Q_{\mathcal{R}_B}(\phi)} \qquad \leq \qquad 1 \qquad (2.21)$$

The probability $P_n m(0)$, for the case where $\theta = \phi$ can be easily evaluated (see appendix A.3), and when it is used to find the marginal probabilities $P_n(\theta)$ and $P_m(\phi)$, they are found to be independent of n and m respectively. When these probabilities are evaluated numerically for varying θ or ϕ, they are found to be also independent of these parameters, so one obtains (see appendix A.3)

$$P_n(\theta) = P_m(\phi) = \frac{1}{N+1} \qquad (2.22)$$

2.4.1   Optimum Analyser Parameters

As the probabilities depend only on the difference between parameters θ and ϕ (2.12), we can define:

$$\chi = \theta - \phi$$

$$\zeta = \theta' - \phi \qquad (2.23)$$

$$\eta = \theta' - \phi'$$

then the Bell inequality becomes dependent on only three parameters:

$$B_{\mathcal{R}}(\chi, \eta, \zeta) = \frac{Q_{\mathcal{R}}(\chi) + Q_{\mathcal{R}}(\eta) + Q_{\mathcal{R}}(\zeta) - Q_{\mathcal{R}}(\chi + \eta - \zeta)}{Q_{\mathcal{R}_{\mathcal{A}}} + Q_{\mathcal{R}_{\mathcal{B}}}} \qquad \leq \qquad 1 \qquad (2.24)$$

Many authors, for example Mermin[22] and Clauser&Shimony[15], when using this inequality on this and other systems with similar properties, choose to focus on the case when

$$\chi = \eta = -\zeta$$

thus having the Bell inequality in the convenient form (using the properties (using (2.24) and the properties (2.13))

$$B_{\mathcal{R}}(\chi) = \frac{3Q_{\mathcal{R}}(\chi) - Q_{\mathcal{R}}(3\chi)}{Q_{\mathcal{R}_{\mathcal{A}}} + Q_{\mathcal{R}_{\mathcal{B}}}} \qquad \leq \qquad 1 \qquad (2.25)$$

However there seems no obvious reason why this should give the best chances of finding any violations for the $N > 1$ case, if they exist.

To find out if these values can be considered optimum, a "brute-force" numerical approach was tried. The ranges $\mathcal{R}_{\mathcal{A}}, \mathcal{R}_{\mathcal{B}}$ of values for which we consider the detectors A, B to record a *count*, were taken to be $n, m > N/2$.[5] Using this range for the *count* result at detectors A and B, the Bell inequality (2.24) (with no noise present $\therefore Q_{\mathcal{R}}(\chi) = P_{\mathcal{R}}(\chi)$) was evaluated at regularly spaced (spacing of $\pi/60$) values of χ, η, ζ in the range

$$-\frac{\pi}{2} \leq \chi, \eta, \zeta \leq \frac{\pi}{2} \qquad (2.26)$$

for several values of N.[6] giving evaluation at $60^3 = 216,000$ points for each N in the 3-dimensional (χ, η, ζ) space.

Note: For larger ranges of χ, η, ζ, $B_{\mathcal{R}}(\chi, \eta, \zeta)$ repeats itself, due to the properties (2.13).

---

[5]This may seem arbitrary, but in later calculations, this is the range which allows violations for the greatest magnitude of noise. Some calculations for determining the optimum range to be included in the $\mathcal{R}$ used here, had to be made using $\chi = \eta = -\zeta$ before this choice of parameters χ, η, ζ was fully justified.

[6]in four separate cacluations, N was taken to be 5, 10, 15 and 20.

It was found that the largest violations were in fact along the line $\chi = \eta = -\zeta$ (perhaps not surprisingly), though other local maxima of $B(\chi, \eta, \zeta)$ did occur, some only marginally smaller than those on $\chi = \eta = -\zeta$. These maxima became more common as N increased, but these subsidiary maxima were always slightly smaller than the main ones.

These results indicate that the search for Bell inequality violation can probably be restricted to looking along $\chi = \eta = -\zeta$, at least for this paticular system[7]. If despite the indications here, some of the subsidiary maxima away from the $\chi = \eta = -\zeta$ line do actually give greater violations (which seems unlikely), these violations would most likely only be marginally greater than those along this line, thus making them insignificant in a search for violation of macroscopic local realism.

All the remaining discussion on higher spin states will concern itself with the case where $\chi = \eta = -\zeta$.

2.4.2 Optimum *Count* Result Range

The next question to be considered concerns the optimum range of n, m values ($\mathcal{R}$) to be treated as a result of *count*. We wish to find the optimum range(s) $\mathcal{R}_\mathcal{A}$ such they allow the Bell inequality (2.25) to be violated for the largest magnitude of noise, i.e. the most macroscopic measurements. There does not seem to be any compelling reason to have the ranges $\mathcal{R}_\mathcal{A}$ and $\mathcal{R}_\mathcal{B}$ different, and this would considerably complicate analysis, so from now on, it will be assumed that $\mathcal{R}_\mathcal{A} \equiv \mathcal{R}_\mathcal{B}$.

Note: It would be easier search for values of $\mathcal{R}_\mathcal{A}$ which give the largest value of $B_\mathcal{R}(\chi)$ with no noise, but this is not exactly what we are looking for, and does actually give different results. (The greatest values of noiseless $B_\mathcal{R}(\chi)$ are found as $\mathcal{R}_\mathcal{A}, \mathcal{R}_\mathcal{B} : n, m \in [L_N, N]$ as $L_N \to N$), but when this range is used, the violations are destroyed very quickly as noise amplitude increases.)

The higher spin state was analysed by Munro and Reid[31], looking for violations of the Bell inequality in the noiseless case. They found that the greatest violations occurred when they took

---

[7]The results of Appendix B.2 are also compatible with this view, although they do not apply strictly for higher spin systems with $N > 1$.

the ranges $\mathcal{R_A}, \mathcal{R_B}$ to be

$$\mathcal{R_A} \equiv \lim_{L_N \to 0}[N - L_N, N] \tag{2.27}$$

This is compatible with the work of Drummond[25]. Using the properties (2.13), paticularily $P_{N-n,N-m}(\chi) = P_{nm}(\chi)$, we see that the range

$$\mathcal{R_A} \equiv \lim_{L_N \to 0}[0, L_N] \tag{2.28}$$

will give the same results as (2.27). This seems to indicate that the regions that give the best violation of the inequality will contain the region near $n = 0$ as part of the range $\mathcal{R_A}$ of n values to be treated as a result of *count*.

To check this more thoroughly, three systems with $N = 5, 10, 20$ respectively were considered. The range $\mathcal{R_A}$ was taken to be between the upper and lower limits K_N and L_N, where allowing for noise in the measurements, K_N, L_N can take on any real values from $-\infty$ to ∞.[8]

$$\mathcal{R_A} \quad : \quad x \in [K_N, L_N]$$
$$\mathcal{R} \equiv (\mathcal{R_A} \otimes \mathcal{R_A}) \tag{2.29}$$
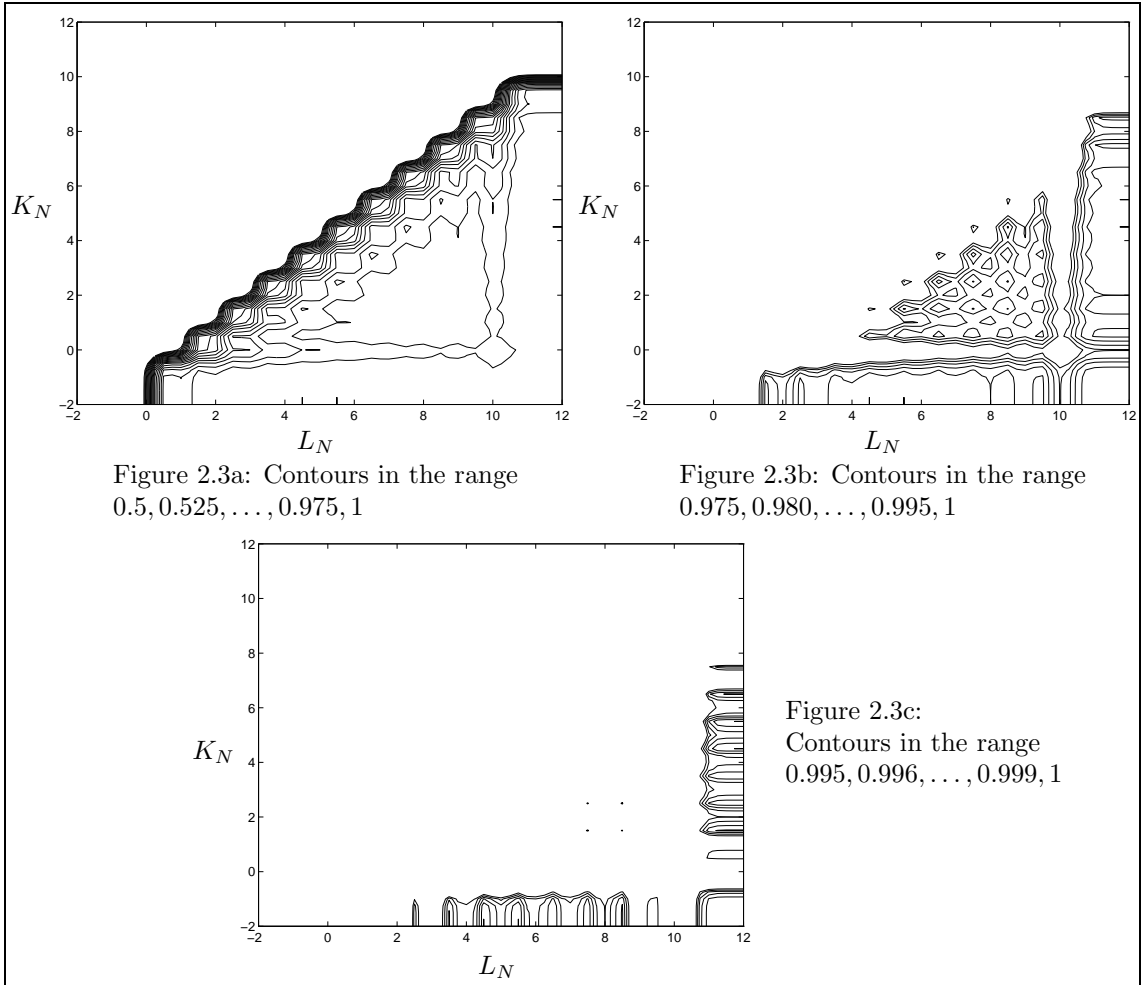
Initially, K_N was taken to be $-\infty$ as considered by Munro and Reid, and L_N was varied between 0 and ∞. For each value of L_N considered, the maximum noise (gaussian) σ_{MAX} that gave a violation of the Bell inequality (2.25) (with optimum values of χ, depending on N and L_N, for each calculation) was calculated. In all three cases, the optimum values of L_N were found to be $L_N = \frac{N}{2} \pm \frac{1}{2}$. Now that an estimate for the maximum noise magnitude has been obtained, we check whether a greater noise magnitude can be introduced while still preserving $B \geq 1$, by varying K_N. To this end, the quantity B (LHS of Bell inequality (2.25)) is evaluated for varying values of K_N and L_N, while keeping $\sigma = \sigma_{\text{MAX}}$ constant. The results of this calculation for $N = 10$ are shown in figure 2.3, where it can be seen that $B < 1$ for all K_N, L_N values except for $K_N = -\infty$ *and* $L_N = \frac{N}{2} \pm \frac{1}{2}$ and the equivalent[9] $K_N = N/2 \pm \frac{1}{2}$ *and* $K_L = \infty$. This indicates

---

[8]the case considered by Munro and Reid had $K_N = 0$ for the noiseless case, which is equivalent to $K_N = -\infty$ when noise is being considered.

[9]These ranges are equivalent in terms of the values of $B(\chi)$ that are obtained when they are used to calculate the probabilities of obtaining a measurement of *count*

Figure 2.3: Variation of the maximum value of $B(\chi)$ (LHS of Bell inequality) for (gaussian) noise standard deviation $\sigma_{\text{MAX}} = 0.38675$ at $N = 10$ with range parameters L_N, K_N. The range is taken to be $\mathcal{R}_\mathcal{A} \equiv n \in [K_N, L_N]$. B is evaluated for optimum analyser parameter χ which varies with L_N, K_N. Note that B only reaches unity for $K_N \to -\infty$, $L_N = 5 \pm \frac{1}{2}$, and the corresponding value $L_N \to \infty$, $K_N = 5 \pm \frac{1}{2}$. B is plotted as a contour plot.

Note: Since *noiseless* measurements can only give values between 0 and N, L_N, K_N values of -2 or 12 are effectively $-\infty$ or ∞ respectively. This is because to get a noisy measurement of 12 or -2 here, one would have to get gaussian noise of about 5 standard deviations magnitude, which is very rare — thus $K_N = -2$(say) gives the same results as $K_N = -\infty$ would.

Figure 2.3a: Contours in the range $0.5, 0.525, \ldots, 0.975, 1$

Figure 2.3b: Contours in the range $0.975, 0.980, \ldots, 0.995, 1$

Figure 2.3c: Contours in the range $0.995, 0.996, \ldots, 0.999, 1$

that other K_N, L_N values do not even allow the noise magnitude to reach σ_{MAX}, so they are sub-

optimal, and can be taken out of consideration. In further calculations, the ranges for n, m used

will be

$$L_N = (N \operatorname{div} 2) + \tfrac{1}{2}$$

$$\mathcal{R_A} \equiv [-\infty, L_N] \tag{2.30}$$

$$\mathcal{R} \equiv \mathcal{R_A} \otimes \mathcal{R_A}$$

where the function div has been previously defined in (2.11).

2.4.3 Noise Simulation

Macroscopic noise tends to be gaussian in nature, so this is the type of noise that the analysis focuses on. To account for the (unlikely) case that gaussian noise is somehow a special case which just happens to not violate the macroscopic Bell inequality, two other forms of noise were tried in the calculations that follow.

As the detectors A and B are separated by a spacelike interval at the time of the measurement, the noise in the n measurement must be independent of the m measurement. Thus we can write

$$\varrho(\Delta_n, \Delta_m) = \rho(\Delta_n)\rho(\Delta_m) \tag{2.31}$$

The gaussian noise distribution can be written (using the notation of section (2.3)) where σ is the standard deviation of the distribution

$$\rho_G(\Delta) = \frac{1}{\sigma\sqrt{2\pi}} \exp\left[\frac{-\Delta^2}{2\sigma^2}\right] \tag{2.32}$$

The other distributions used were a "box" and a "triangular" distribution as given below.

$$\text{BOX:} \qquad \rho_B(\Delta) = \begin{cases} \dfrac{1}{2a} & \text{for} \quad -a < \Delta < a \\[2mm] 0 & \text{otherwise} \end{cases} \tag{2.33}$$

This noise has a box-shape, of width $2a$ and standard deviation $\dfrac{a}{\sqrt{3}}$.

$$\text{TRIANGLE:} \qquad \rho_T(\Delta) = \begin{cases} \dfrac{b+x}{b^2} & \text{for} \quad -b < \Delta \leq 0 \\[2mm] \dfrac{b-x}{b^2} & \text{for} \quad 0 < \Delta < b \\[2mm] 0 & \text{otherwise} \end{cases} \tag{2.34}$$

Figure 2.4: Noise distributions used to simulate macroscopic measurements on the higher spin state. $\rho(\Delta)$ is the probability density that any paticular measurement is changed by Δ from the noiseless value that would be measured with ideal apparatus. Gaussian, "Box" and "Triangular" distributions are shown. Δ is given in units of $\sigma = 1$ standard deviation.

Δ in σ units	Δ in σ units	Δ in σ units
Figure 2.4a: Gaussian Noise	Figure 2.4b: "Box" Noise. $a = \sqrt{3}\sigma$	Figure 2.4c: "Triangular" Noise. $b = \sqrt{6}\sigma$
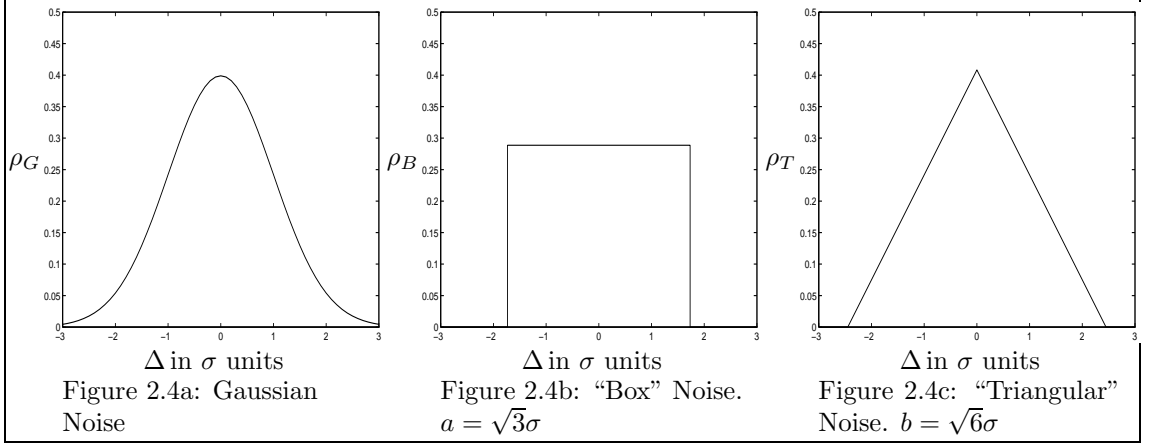
This noise has a triangle-shape, of width $2b$ and standard deviation $\dfrac{b}{\sqrt{6}}$

These distributions are displayed in figure 2.4. As mentioned in section 2.4.2, the optimum range $\mathcal{R}$ ($\equiv \mathcal{R}_{\mathcal{A}} \otimes \mathcal{R}_{\mathcal{B}}$) which gives the most "macroscopic" violations for this state (2.6) is the range $x, y \in [-\infty, L_N]$. For this range, the "noise coefficients" mentioned in section 2.3 can be evaluated. They are found to be

$$\text{GAUSSIAN:} \quad C_n^G(\sigma, L_N) = \frac{1}{\sqrt{\pi}} \int_{-\infty}^{\frac{L_N - n}{\sigma\sqrt{2}}} \exp\left[-z^2\right]\, dz \tag{2.35}$$

$$\text{(which is the well known Error function)}$$

$$\text{BOX:} \quad C_n^B(a, L_N) = \begin{cases} 0 & \text{if } n > L_N + a \\ 1 & \text{if } n < L_N - a \\ \dfrac{1}{2} + \dfrac{1}{2}\left(\dfrac{L_N - n}{a}\right) & \text{otherwise} \end{cases} \tag{2.36}$$

$$\text{TRIANGLE:} \quad C_n^T(b, L_N) = \begin{cases} 0 & \text{if } n > L_N + b \\ 1 & \text{if } n < L_N - b \\ \dfrac{1}{2} + \dfrac{L_N - n}{b} - \dfrac{1}{2}\,\text{sign}[L_N - n]\left(\dfrac{L_N - n}{b}\right)^2 & \text{otherwise} \end{cases} \tag{2.37}$$

2.4.4 Maximum Bell-Inequality-Violating Noise

Finally, we come to the main issue for the higher spin states: how large can we make the noise before any violations of the Bell inequality are destroyed? It turns out that the maximum noise

magnitude (corresponding to noise standard deviation $\sigma_{\mathrm{MAX}}(N)$) is slightly above 0.4 bosons for large N, and less for small N.

The results are summarised in more detail in table 2.1, and the maximum noise parameters $\sigma_{\mathrm{MAX}}(N), a_{\mathrm{MAX}}(N), b_{\mathrm{MAX}}(N)$ are shown as a function of N in figure 2.6. A plot of maximum violation (if any) of the Bell inequality as a function of N, for several values of noise magnitude, is also given in figure 2.5. It was found that the noise could be made slightly larger for odd N than for even N (by about 0.006 as $N \to \infty$), but this is certainly an unimportant mathematical detail due to the fact that $\sigma_{\mathrm{MAX}} < 1$. Since the range boundaries L_N were placed at half-integral values, any noise of less than 0.5 standard deviation is basically insignificant. It is in fact found that if $\mathcal{P}_{0.5}$ is the probability that the noise changes the result of a measurement at a detector from its noiseless value by more than $\frac{1}{2}$, then when $\mathcal{P}_{0.5} > 0.228$ (0.221 for even N), any Bell inequality violations are swamped by the noise. This applies equally to all three forms of noise considered. The procedure used to obtain these results is discussed below.

Table 2.1: Maximum Bell-inequality-violating noise parameters $\sigma_{\mathrm{MAX}}, a_{\mathrm{MAX}}, b_{\mathrm{MAX}}$ observed for the higher spin systems as $N \to \infty$.

Noise Type	Parameter name	Max. value	Standard deviation
Gaussian	σ_{MAX}	0.4146	0.4146
"Box"	a_{MAX}	0.6478	0.3740
"Triangular"	b_{MAX}	0.9573	0.3908

The measured quantities for the higher spin state are the boson numbers n, m. The probabilities in the Bell inequality (2.25) — $Q_{\mathcal{R}}(\chi)$ are the probabilities that the results (x, y) of noisy n, m measurements are within the range $\mathcal{R} = \mathcal{R}_{\mathcal{A}} \otimes \mathcal{R}_{\mathcal{A}}$, where

$$\mathcal{R}_{\mathcal{A}} \equiv \left[-\infty, N \operatorname{div} 2 - \tfrac{1}{2}\right] \tag{2.38}$$

For each value of N considered, the maximum noise magnitudes which give violations of (2.25) were found to within an error 0.001 for each of the three types of noise considered in section 2.4.3. To calculate the LHS of the Bell inequality, $B_{\mathcal{R}}(\chi)$, the probability distribution $P_{nm}(\chi)$ of obtaining a noiseless measurement of n bosons at detector A, and m bosons at detector B

Figure 2.5:
Maximum violation of the Bell inequality B_{MAX} against number of bosons N for several simulated noise magnitudes. The Bell inequality is violated for $B_{\text{MAX}} > 1$. In all cases, the value B_{MAX} shown is B evaluated at $\chi = \chi_{\text{MAX}}$ which maximises $B(\chi)$. The uncertainty in B_{MAX} is less than ± 0.00005 which is less than the size of the symbols used to show data. Noise used is gaussian in form. Different symbols show data for different magnitudes(i.e. standard deviations) of noise. $+$: no noise, $\circ$: $\sigma = \frac{1}{2}$, $\times$: $\sigma = 1$.
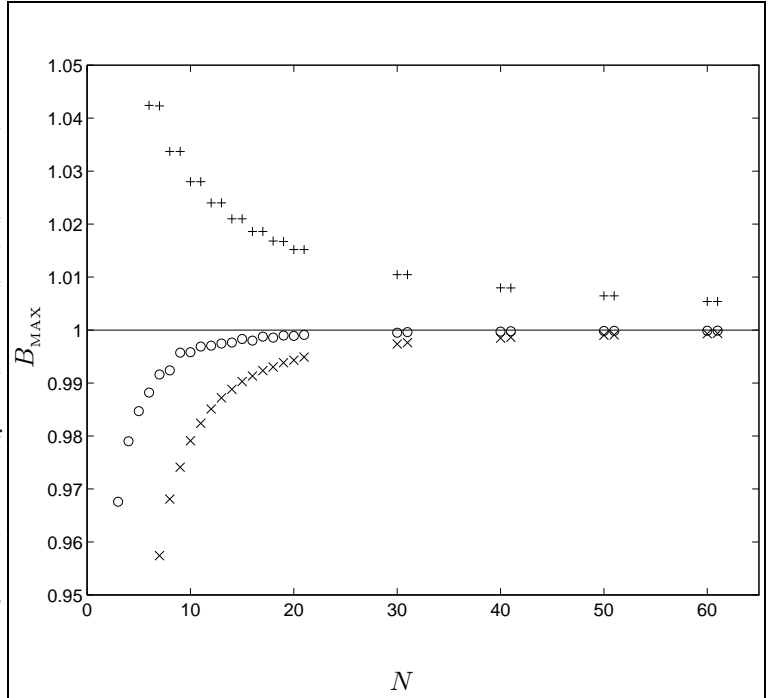
was calculated exactly, for 120 values of χ in the range $\chi, \chi + \frac{\pi}{480}, \ldots, \frac{\pi}{4}$. These values were then used to approximate $P_{nm}(\chi)$ for arbitrary χ using a cubic polynomial interpolation method, and the properties (2.13). These approximate noiseless values were used to calculate the noisy probabilities of measuring a *count* event $Q_{\mathcal{R}}(\chi)$ for a given noise distribution and arbitrary χ (using the equations (2.19), (2.20), (2.35)–(2.37)) . The marginal probabilities $Q_{\mathcal{R}_{\mathcal{A}}}$ and $Q_{\mathcal{R}_{\mathcal{B}}}$ are given by (2.22) and (2.38) to be

$$Q_{\mathcal{R}_{\mathcal{A}}} = Q_{\mathcal{R}_{\mathcal{B}}} = \frac{N \operatorname{div} 2 + \frac{1}{2}}{N + 1} \tag{2.39}$$

Thus the Bell inequality (2.25) was evaluated, and maximum noise magnitudes were calculated by a numerical minimising procedure with error tolerance 0.5×10^{-4} (minimising $|B(\chi_{\text{MAX}}, \sigma) - 1|$).[10] The calculated values are shown in figure 2.6.

A question now arises whether sampling 120 values in the range 0 to $\frac{\pi}{4}$ is sufficient to obtain an accuracy of similar order to the minimising procedure (0.5×10^{-4}) for the approximation to $P_{nm}(\chi)$ and eventually for $B_{\mathcal{R}}(\chi)$. To test the accuracy of such approximations, the same

---

[10]χ_{MAX} is the χ value at which B is maximised

Figure 2.6: Maximum simulated noise amplitudes, which still allow the higher spin state to violate the Bell inequality. Data points have uncertainty $\pm 5 \times 10^{-4}$ or less. N varies between 1 and 61. Parameters for odd N are marked as circles ($\circ$), even N as stars ($*$). All data points are accurate to within about $\pm 5 \times 10^{-4}$, which is much less than the size of the symbols used to display them.

Figure 2.6a: Gaussian noise. Maximum standard deviation $= \sigma_{\text{MAX}}(N)$. As $N \to \infty$, $\sigma_{\text{MAX}}(N) \to 0.4145 \pm 0.0005$ for odd N and to 0.4085 ± 0.0005 for even N.

Figure 2.6b: "Box" noise. Maximum standard deviation $= a_{\text{MAX}}(N)/\sqrt{3}$. As $N \to \infty$, $a_{\text{MAX}}(N) \to 0.6480 \pm 0.0005$ for odd N and to 0.6420 ± 0.0005 for even N.

Figure 2.6c: "Triangular" noise. Maximum standard deviation $= b_{\text{MAX}}(N)/\sqrt{6}$. As $N \to \infty$, $a_{\text{MAX}}(N) \to 0.9570 \pm 0.0005$ for odd N and to 0.9440 ± 0.0005 for even N.
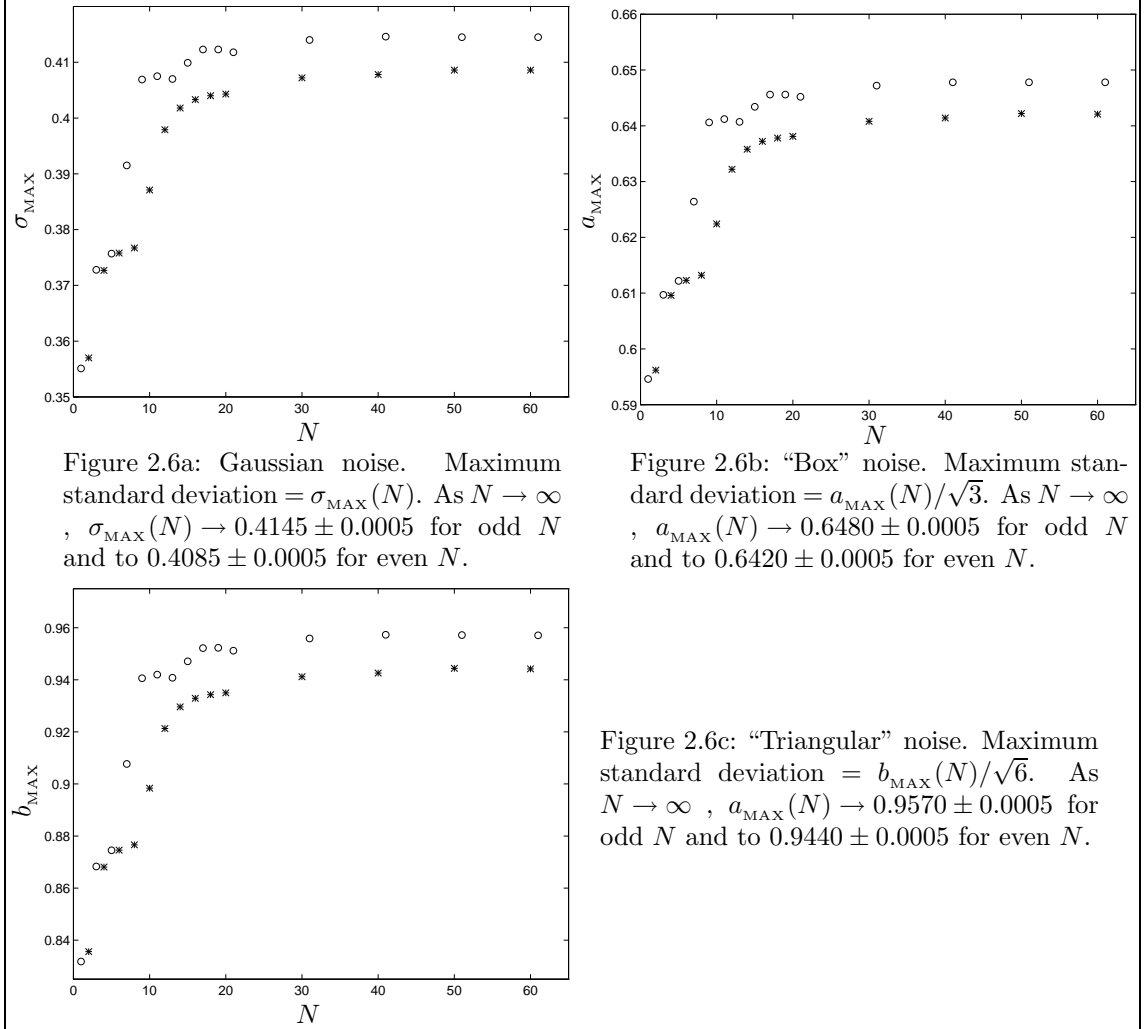
procedure outlined above was repeated for some values of N, using smaller "resolution" in χ, such as 30 or 60 values between 0 and $\frac{\pi}{4}$. The results were found to agree to within 0.0005 or better as long as the "resolution", *number of steps* was significantly less than N. When *number of steps* approached or exceeded N, the lower resolution calculations generally overestimated the maximum noise parameter. By these results, it is fair to conclude that the maximum standard deviations and noise parameters $\sigma_{\text{MAX}}, a_{\text{MAX}}, b_{\text{MAX}}$ for the gaussian, "box" and "triangular" noise distributions, for any given N are accurate to within at least 0.0005 if *number of steps* is significantly less than

N. This is the case for the calculations discussed above for $N \lesssim 60$. For $N > 60$, the *number of steps* must be increased again, making calculations more laborious.

2.5 Conclusions for Higher Spin States

A fairly exhaustive search for Bell inequality violations was carried out on the higher spin states (2.6) by varying the parameters θ, ϕ, and the *count* range (see subsection 2.4.2). It seems unlikely that any significant[11] violations of the Bell inequality were missed, although this admittedly remains a possibility. On the basis of the violations that were found, it seems very unlikely that any violations of the Bell inequality can happen when the noise in the experiment is ± 0.5 photons or more. As the measured quantities here are particle numbers, noise this small is almost un-noticeable, and is most certainly of a microscopic nature.

Thus it can be concluded that although the quantum mechanical predictions for the higher spin states aare incompatible with microscopic local realism, they most probably *do not* violate macroscopic local realism.

---

[11]i.e. violations of the Bell inequality that would show different behaviour to that seen in figure 2.6, as noise magnitude was increased

Chapter 3

The "Circular" Superposition of Coherent States

The state considered here (see section 3.1 below) is a superposition of coherent states shown by Reid and Krippner[14] to be (potentially) generated in lossless nondegenerate parametric oscillation above threshold. Here we will be considering two modes $\hat{a}$ and $\hat{b}$. The states considered are eigenstates of the photon number difference $\hat{b}^\dagger \hat{b} - \hat{a}^\dagger \hat{a}$.

This state is referred to as "circular" as it consists of a superposition of coherent states of the same amplitude, but varying phase. When the complex parameters α of the coherent states ($|\alpha\rangle$) in the superposition are plotted in the complex plane, the locus is a circle.

States consisting of superpositions of coherent states seem to be good candidates in which to look for possible violations of macroscopic local realism for at least two reasons.

- Coherent states can be produced relatively easily using lasers. Thus states containing them may be easier to produce in practice than many other kinds.

- Quadrature phase measurements are possible on light fields, among them coherent states. The attraction of quadrature phase measurements is that when they are measured via a

homodyne detection scheme[34], by assuming *local realism*[1], the elements of reality can be defined[9] to correspond to measured quantities which are proportional to the amplitude of a so-called "local oscillator field", which is a high-intensity macroscopic light field. The amplitude of this field can theoretically be increased at will, until any macroscopic noise sources present are too small to affect the violation or non-violation of the Bell inequality.[2] Thus here, any significant violation of the Bell inequality can probably be made macroscopic.

Violations of the Bell inequality were indeed found (see section 3.3).

3.1 The State

The state being considered is:

$$|\psi\rangle = \frac{e^{r^2} \int_0^{2\pi} \left|re^{i\mu}\right\rangle_A \left|re^{-i\mu}\right\rangle_B \, d\mu}{2\sqrt{\pi \int_0^\pi \exp\left[2r^2\cos(\omega)\right] \, d\omega}} \tag{3.1}$$

where $\left|re^{i\mu}\right\rangle_A$ is a coherent state of mean photon number r^2, and phase μ in spatial region A. $\left|re^{-i\mu}\right\rangle_B$ is defined similarily, as a coherent state with identical photon number r^2 and correlated phase $-\mu$, in a spatially separated region B.

$\int_0^\pi \exp\left[2r^2\cos(\omega)\right] \, d\omega$ is a constant normalisation factor, dependent only on r, which can be calculated numerically. It can be shown that

$$\int_0^\pi \exp\left[2r^2\cos(\omega)\right] \, d\omega = \pi \sum_{i=0}^\infty \frac{r^{4i}}{(i!)^2} \tag{3.2}$$

This state corresponds to a source producing an entangled quantum superposition of a large number of different pairs of coherent states.

A homodyne detector with local oscillator field magnitude ε and phase θ is placed in region A to measure $\hat{x}(\theta)$, a quadrature phase operator of the field in region A. Another homodyne detector with local oscillator phase ϕ and the same magnitude ε is placed in region B, to measure $\hat{y}(\phi)$

---

[1]see section 1.5

[2]Assuming of course, that the magnitude of the macroscopic noise present is not proportional to the amplitude of the local oscillator field.

Figure 3.1: A schematic diagram of the experimental setup for the "circular" superposition of coherent states (3.1). Spatially separated superpositions of correlated coherent states are created at the source and move to regions A, B where the quadrature phase operators $\hat{x}, \hat{y}$ are measured by homodyne detectors. The local oscillator phases θ, ϕ are the adjustable experimental parameters. Here ε^2 is the local oscillator photon number.
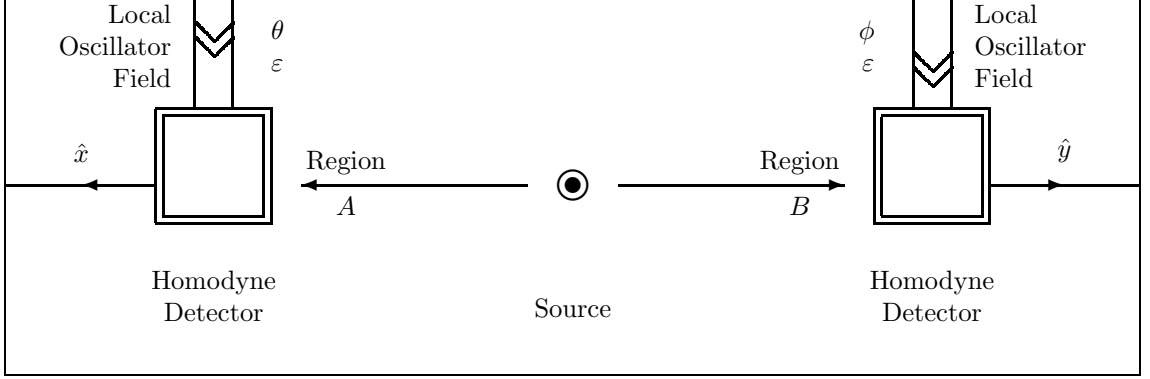
the quadrature phase operator of the second field in region B. θ, ϕ are parameters which can be varied by the experimenter at will. These correspond to the parameters a, b in the generalised Bell inequality (1.5). The operators $\hat{x}, \hat{y}$ have continuous eigenvalues. This situation is shown in figure 3.1.

Note: The operators that are *actually* measured are $\hat{X}_\varepsilon(\theta), \hat{Y}_\varepsilon(\phi)$ given by $\hat{X}_\varepsilon(\theta) = \varepsilon\hat{x}(\theta)$ and

$\hat{Y}_\varepsilon(\phi) = \varepsilon\hat{y}(\phi)$, where ε is the classical amplitude of the local oscillator field, a constant (the number of photons in the local oscillator field is ε^2). Thus $\hat{x}, \hat{y}$ can be implied from measurements of $\hat{X}, \hat{Y}$.

The quadrature phase operators that will be considered here are

$$\hat{x}(\theta) = \tfrac{1}{\sqrt{2}}\left[e^{i\theta}\hat{a} + e^{-i\theta}\hat{a}^\dagger\right] \qquad\qquad \hat{X}_\varepsilon(\theta) = \varepsilon\hat{x}(\theta) \qquad (3.3)$$

$$\hat{y}(\phi) = \tfrac{1}{\sqrt{2}}\left[e^{-i\phi}\hat{b} + e^{i\phi}\hat{b}^\dagger\right] \qquad\qquad \hat{Y}_\varepsilon(\phi) = \varepsilon\hat{y}(\phi) \qquad (3.4)$$

where $\hat{a}, \hat{a}^\dagger$ are anihilation and creation operators on the field in region A, and $\hat{b}, \hat{b}^\dagger$ are analogous operators in region B. There is no significance attached to the fact that in the expression above, θ corresponds to $-\phi$ not ϕ if the operators $\hat{x}, \hat{y}$ are put into the same form. This is introduced purely for convenience in changing to the $\hat{x}$-$\hat{y}$ representation, (see section 3.2 below).

3.2 The Measured Quantities

The quantities to be measured and analysed here are the magnified quadrature phase operators $\hat{X}(\theta) = \varepsilon\hat{x}(\theta), \hat{Y}(\phi) = \varepsilon\hat{y}(\phi)$. The x, y representation of $|\phi\rangle$ can be found by use of the expression[35]

$$\langle x| \alpha\rangle = \pi^{-\frac{1}{4}} \exp\left[-\frac{x^2}{2} - \frac{|\alpha|^2}{2} + \sqrt{2}x\alpha e^{i\theta} - \frac{\alpha^2 e^{2i\theta}}{2}\right] \tag{3.5}$$

where $|\alpha\rangle$ is a coherent state, and $|x\rangle$ is an eigenstate of the operator $\hat{x} = \frac{1}{\sqrt{2}}[e^{i\theta}\hat{a} + e^{-i\theta}\hat{a}^\dagger]$ with eigenvalue x ($\hat{a}$ is an anihilation operator on the photon field).

The probability density of measuring the value x for the operator $\hat{x}$ in region A, and the value y for the operator $\hat{y}$ in region B is given by

$$P_{xy}(\theta, \phi) = \langle x|_A \langle y|_B |\psi\rangle \langle\psi| |x\rangle_A |y\rangle_B = \Psi^*_{xy}(\theta, \phi)\Psi_{xy}(\theta, \phi) \tag{3.6}$$

where $|x\rangle_A$ is an eigenvector of the operator $\hat{x}$ in region A defined in (3.3), with eigenvalue x. Via (3.5) it can be shown[3] that

$$\Psi_{xy}(\chi) = \frac{\exp\left[\frac{x^2+y^2}{2}\right]}{2\pi\sqrt{\int_0^\pi \exp\left[2r^2\cos(\omega)\right]\,d\omega}} \int_0^{2\pi} \exp\left[-\left(\frac{r}{\sqrt{2}}e^{i\mu} - x\right)^2 - \left(\frac{r}{\sqrt{2}}e^{i\chi}e^{-i\mu} - y\right)^2\right]\,d\mu \tag{3.7}$$

which is only dependent on $\chi = \theta - \phi$, the difference between the two instrument parameters, not θ and ϕ separately. Thus we also have $P_{xy}(\chi)$, dependent on χ only. This integral can be evaluated numerically. This probability distribution is shown graphically in figure 3.2.
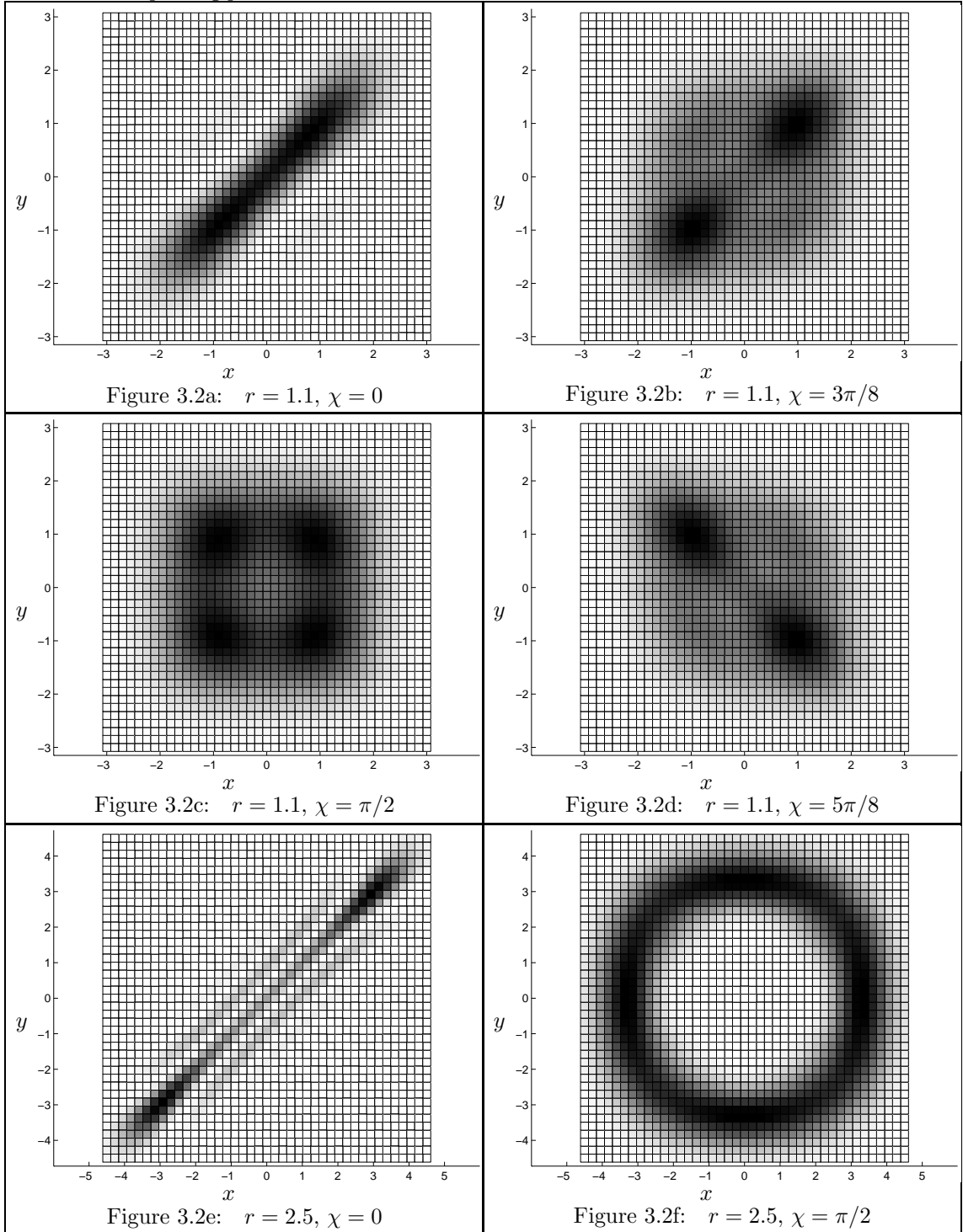
The marginal probability density of measuring the operator $\hat{x}$ at A to be x, irrespective of the measurement of $\hat{y}$ at B is given by

$$P_x(\theta) = \int_{-\infty}^{\infty} P_{xy}(\theta, \phi)\,dy \tag{3.8}$$

and analogously for $\hat{y}$ at B.

---

[3]see Appendix B.1

Figure 3.2: Probability distributions for the "circular" superposition of coherent states (3.1). Figures show variation of probability density $P_{xy}(\chi)$ with parameter χ. The top four figures are for coherent state amplitudes $r = 1.1$ near which the maximum Bell inequality violations are observed. The bottom two figures are for $r = 2.5$. Dark shading indicates high probability density. Note that the magnitude of the probability represented by a given shading varies between plots, and that the grid lines are non-significant artefacts of the plotting process.

Figure 3.2a: $r = 1.1$, $\chi = 0$

Figure 3.2b: $r = 1.1$, $\chi = 3\pi/8$

Figure 3.2c: $r = 1.1$, $\chi = \pi/2$

Figure 3.2d: $r = 1.1$, $\chi = 5\pi/8$

Figure 3.2e: $r = 2.5$, $\chi = 0$

Figure 3.2f: $r = 2.5$, $\chi = \pi/2$

3.3   Testing of the Bell Inequality

We have the Bell inequality (1.5)

$$\frac{P_{AB}(a,b) + P_{AB}(a',b) + P_{AB}(a',b') - P_{AB}(a,b')}{P_A(a') + P_B(b)} \leq 1$$

where now a, b correspond to θ, ϕ, and P_{AB} corresponds[4] to $P_{\mathcal{R}}$, the probability of obtaining a measurement of *count*, defined by the range $\mathcal{R}$ of x, y values that are considered to be a result of *count*. Thus $P_{AB}(a,b) \rightarrow P_{\mathcal{R}}(\chi)$.

It is found numerically that the marginal probability densities $P_x(\theta)$ and $P_y(\phi)$ are independent of the parameters θ, ϕ respectively.

Thus as in subsection 2.4.1 one can define (2.23)

$$\chi = \theta - \phi$$

$$\zeta = \theta' - \phi \qquad \qquad (3.9)$$

$$\eta = \theta' - \phi'$$

and simplify the Bell inequality to

$$B_{\mathcal{R}}(\chi, \eta, \zeta) = \frac{P_{\mathcal{R}}(\chi) + P_{\mathcal{R}}(\eta) + P_{\mathcal{R}}(\zeta) - P_{\mathcal{R}}(\chi + \eta - \zeta)}{P_{\mathcal{R}_{\mathcal{A}}} + P_{\mathcal{R}_{\mathcal{B}}}} \qquad \leq \qquad 1 \qquad (3.10)$$

similarily to (2.21) in chapter 2.

To test the Bell inequality with some chance of success, we must find a reasonable range of measured values x, y to consider as a result of *count*, and determine suitable values of the parameters χ, η, ζ to search for violations, as an exhaustive "brute-force" search would be too time consuming[5].

---

[4]using the notation of section 1.7

[5]This applies to this state more than for the higher spin states considered in chapter 2, as the probability densities (3.7) here are not expressible as analytical functions, and are continuous. This means that to calculate $P_{\mathcal{R}}(\chi)$ (say), a triple numerical integration must be performed. This can become very time consuming if resonable accuracy is to be achieved.

3.3.1 Choice of *Count* Range

It was chosen to make the range $\mathcal{R}$ of x, y values, to be regarded as a result of *count*, the positive quadrant on the x-y plane. i.e. using the notation of section 1.7 we have the range $\mathcal{R}$:

$$\mathcal{R}_\mathcal{A} = \mathcal{R}_\mathcal{B} \quad \equiv \quad [0, \infty] \tag{3.11}$$

$$\mathcal{R} = \mathcal{R}_\mathcal{A} \otimes \mathcal{R}_\mathcal{B} \tag{3.12}$$

This range was chosen for a number of reasons. From least to most important:

- An analogous range (2.30) covering a quadrant of the x-y plane of measured quantities, was found to be the optimum range for the higher spin states considered in chapter 2.

- Inspection of the probability densities for the states (figure 3.2) indicates that $P_{xy}(0)$, the probability density at $\chi = 0$ is clumped in two regions in the positive and negative quadrants of the x-y plane that quickly become better separated as the coherent state amplitude r increases. This corresponds to an intuitive concept of an "element of reality".

- Most importantly, this range gives a "local maximum" of the LHS of the Bell inequality B. i.e. If the range $\mathcal{R}$ is varied by

   - expanding its lower bound (to negative x, y values),

   - shrinking its lower bound (disallowing some small positive x, y values)

   - shrinking its upper bound (disallowing some large x, y values)

   - making it unsymmetric in x and y (making $\mathcal{R}_\mathcal{A} \not\equiv \mathcal{R}_\mathcal{B}$)

   then the magnitude of B decreases. ($B > 1$ is needed for a violation of the Bell inequality).

This choice of $\mathcal{R}$ does in fact produce significant violations of the Bell inequality (see subsection 3.3.3) given the right choice of parameters χ, η, ζ (see below). Other range choices might also give violations, prehaps greater than those observed, but this was not investigated due to time constraints.

When the marginal probabilities $P_x(\theta), P_y(\phi)$ are evaluated numerically, they are found to be constant (independent of the parameters θ, ϕ). Additionally, when the ranges given above in (3.11) are used, the marginal probabilities are equal to half.

$$P_{\mathcal{R}_\mathcal{A}} = P_{\mathcal{R}_\mathcal{B}} = \tfrac{1}{2} \tag{3.13}$$

3.3.2   Choice of Parameters

Consider the Bell inequality that will be used here (3.10). To violate the inequality it is required that (as the marginal probabilities are given by (3.13))

$$B_\mathcal{R}(\chi, \eta, \zeta) = P_\mathcal{R}(\chi) + P_\mathcal{R}(\eta) + P_\mathcal{R}(\zeta) - P_\mathcal{R}(\chi + \eta - \zeta) \quad > \quad 1 \tag{3.14}$$

It can be shown (see appendix B.2) that for some functions $P(\chi)$ if $B = P(\chi) + P(\eta) + P(\zeta) - P(\chi + \eta - \zeta)$ and

$P(\chi)$ is periodic in χ with period L (3.15)

$P(\chi)$ has three extrema per period: maxima at $\chi = 0, L$ and a minimum at $\chi = \dfrac{L}{2}$ (3.16)

$P(L - \chi) = P(\chi)$ for all χ (3.17)

$\dfrac{\partial P(\chi)}{\partial \chi} = P'(\chi)$ has only three extrema in the range $0 \leq \chi \leq \tfrac{L}{2}$ (3.18)

   (maxima at $\chi = 0, \tfrac{L}{2}$ and a minimum in between)

then B will attain its greatest value above 2P(0) (if any) on the line in χ, η, ζ space given by

$$\chi = \eta = -\zeta$$
$$0 \leq \chi, \eta \leq \tfrac{L}{2} \tag{3.19}$$
$$-\tfrac{L}{2} \leq \zeta \leq 0$$

Furthermore, if

$$P'(\tfrac{L}{2} - \chi) = P'(\chi) \tag{3.20}$$

then the greatest value of B will be attained at one or both of

$$\chi = \eta = \frac{L}{8} \text{ or } \frac{3L}{8} = -\zeta \tag{3.21}$$

This is very useful, as an exhaustive search of the various angles χ, η, ζ is not required. When $P_{\mathcal{R}}(\chi)$ is calculated numerically, it is found to always satisfy conditions (3.15)-(3.17) and (3.20), and to satisfy condition (3.18) if r is small (i.e. less than about 1.5). The period is found to be $L = 2\pi$, and $P_{\mathcal{R}}(0) = 0.5$.

Thus for low r, violations of the Bell inequality were checked only for the parameters

$$\chi = \eta = \frac{\pi}{4} \text{ or } \frac{3\pi}{4} = -\zeta. \tag{3.22}$$

The case where $\chi = \frac{3\pi}{4}$ was found to always be a minimum of B and thus irrelevant for our purposes here. Thus for violations of the Bell ineqaulity we require

$$B_{\text{MAX}} = 3P_{\mathcal{R}}\left(\frac{\pi}{4}\right) - P_{\mathcal{R}}\left(\frac{3\pi}{4}\right) \quad > \quad 1 \tag{3.23}$$

3.3.3 Violations of the Bell Inequality Found

Using the range $\mathcal{R}$ given above in (3.11) and the relation (3.23) required for violation of the Bell inequality, it was found that the Bell inequality was violated by the state 3.1 for r values in the range

$$0.96 \lesssim r \lesssim 1.41 \tag{3.24}$$

The maximum violation of $B_{\text{MAX}} \approx 1.0157 \pm 0.0002$ being around $r \approx 1.1$. A plot of maximum violation B_{MAX} is shown in figure 3.3. The procedure used to obtain this result is outlined below.

To calculate B_{MAX} via (3.23) $P_{\mathcal{R}}(\frac{\pi}{4})$ and $P_{\mathcal{R}}(\frac{3\pi}{4})$ must be calculated. These are given by (using the range in (3.11))

$$P_{\mathcal{R}}(\chi) = \int_0^\infty \int_0^\infty P_{xy}(\chi) \, dx \, dy \tag{3.25}$$

which requires a numerical integration to calculate $P_{xy}(\chi)$ and then two more to calculate $P_{\mathcal{R}}$. The integration method used was the "Adaptive recursive Newton Cotes 8 panel rule". Each integral calculation involved about 25 steps, thus aiming to get a tolerance of $\pm 5 \times 10^{-5} = \Delta$ for $P_{\mathcal{R}}$ calculations, P_{xy} was calculated to a tolerance of $\pm 0.2 \times 10^{-5} = \frac{\Delta}{25}$, and $\int P_{xy} \, dx$ was calculated to a tolerance of $\pm 1 \times 10^{-5} = \frac{\Delta}{5}$. Now if $P_{\mathcal{R}}$ is calculated to an error of $\pm \Delta$, then B, given by

Figure 3.3:
Maximum violation of the Bell inequality B_{MAX} against coherent state amplitude r. The Bell inequality is violated for $B > 1$. In all cases, maximum violation occurred for parameter $\chi = \frac{\pi}{4}$ where $B(\chi) = 3P_{\mathcal{R}}(\chi) - P_{\mathcal{R}}(3\chi)$. The uncertainty in B_{MAX} is about $\pm\,0.0002$, which is much less than the extent of the "+" used to show data on the plot.
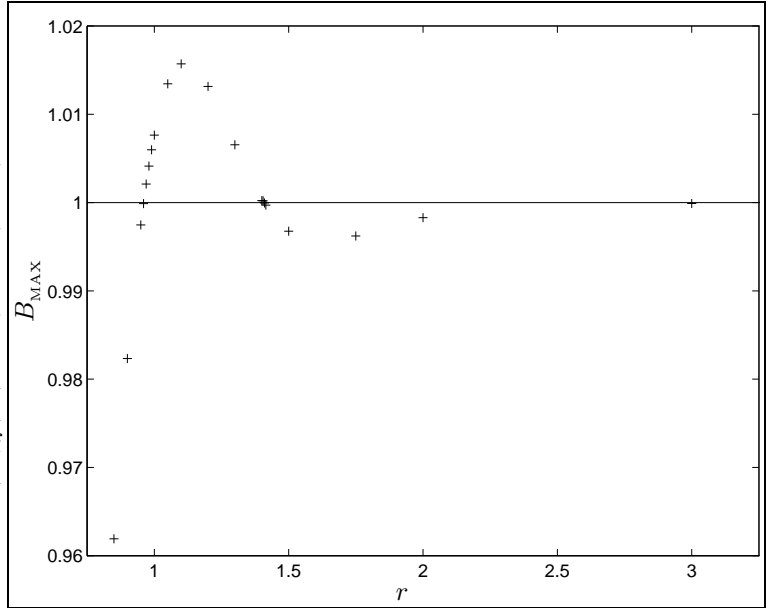
(3.23) will be accurate to about $\pm 3\Delta$, so it was concluded that the calculated values of B_{MAX} were accurate to about $\pm 2 \times 10^{-4}$ leaving plenty of room for the accumulation of error through various steps in the numerical calculations.

Realistically,one cannot integrate to ∞ as is given in (3.25), so the integrations in x and y were done over the range $[0, 2 + r\sqrt{2})$ as it was found that for $x, y \gtrsim 2 + r\sqrt{2}$, $P_{xy}(\chi)$ is negligible for all χ.

This procedure was used to calculate B_{MAX} for all the r values shown in figure 3.3.

3.3.4   Tolerance of the Violations to Noise

It has already been pointed out that the actual measurements, and elements of reality in the hidden variable representation, for this system are the $X, Y = \varepsilon x, \varepsilon y$ from which the values of the standard quadrature phase measurements x, y can be implied if one knows the magnitude ε of the local oscillator field. Thus Bell inequality violations can still occur in the range (3.24) under any magnitude of noise, because if noise magnitude increases, its effect can be countered by increasing ε. Nevertheless, it is interesting to see just how much noise is needed to destroy violations of the Bell inequality for this system.

The following calculations were all performed on the case where $r = 1.1$ which is near the r value which gives the largest inequality violations (i.e. largest B). The noise being considered is gaussian in form, and given by

$$\rho_G(\Delta) = \frac{1}{\sigma\sqrt{2\pi}} \exp\left[\frac{-\Delta^2}{2\sigma^2}\right] \tag{3.26}$$

where the notation of section 2.3 is being used. Here $\rho_G(\Delta)\,d\Delta$ is the probability that the result of a noisy measurement is shifted by the noise by an amount Δ to $\Delta + d\Delta$ from its noiseless value. The probability of measuring a noisy result in the range $\mathcal{R}$ given by $Q_{\mathcal{R}}(\chi)$ can be given by a version of equation (2.19) from section 2.3 modified for continuous noiseless variables:

$$Q_{\mathcal{R}}(\chi) = \iint_{-\infty}^{\infty} P_{xy}(\chi)C_{xy}(\mathcal{R})\,dx\,dy \qquad \text{where} \tag{3.27}$$

$$C_{xy}(\mathcal{R}) = C_x(\mathcal{R}_{\mathcal{A}})C_y(\mathcal{R}_{\mathcal{B}}) \qquad \text{and} \qquad C_x(\mathcal{R}_{\mathcal{A}}) = \iint_{z \in \mathcal{R}_{\mathcal{A}}} \rho_G(z - x)\,dz \tag{3.28}$$

Thus the C_x can be calculated, and $Q_{\mathcal{R}}(\chi)$ is integrated over. The integration was only taken over the x, y ranges $(-4\Delta, 2 + r\sqrt{2})$ as the quantity $Q_{xy} = P_{xy}C_xC_y$ will be negligible outside these bounds.

Proceeding with the above integration in the manner of section 3.3.3, it is found that for $r = 1.1$, Bell inequality violations occur for all noise of magnitude 0.19ε or less. This is shown in figure 3.4.

Figure 3.4:
Maximum violation of the Bell inequality B_{MAX} for coherent state amplitude $r = 1.1$ plotted against gaussian experimental noise magnitude σ. The Bell inequality is violated for all $B_{\mathrm{MAX}} > 1$. In all cases, maximum violation occurred for parameter $\chi = \frac{\pi}{4}$ where $B(\chi) = 3P_{\mathcal{R}}(\chi) - P_{\mathcal{R}}(3\chi)$. The uncertainty in B_{MAX} is about $\pm\,0.0002$, which is much less than the extent of the "+" used to show data on the plot. the horizontal axis = noise magnitude, is given in units of local oscillator field magnitude ε.
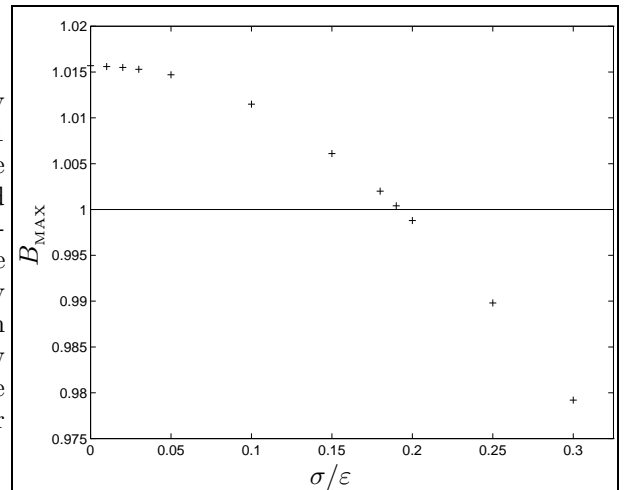
3.4   Conclusions for the "Circular" Superposition of Coherent States

Firstly it should be noted that the hidden variable representation for the state (3.1) considered here, assigns "elements of reality" (as described in section 1.2) to the results of measurements of $X, Y = \varepsilon x, \varepsilon y$ the *amplified* quadrature phase measurements. The quantities X, Y are actually measured as some number of photons in the homodyne detection scheme used here, but usually the local oscillator field magnitude ε is sufficiently large to treat it as an amplifying constant instead of a quantum mechanical operator. In other words, ε is large enough to make the measurement of $X = \varepsilon x$ practically a continuous measurement, as opposed to a discrete photon-number measurement. Therefore we can treat ε as an amplifying constant on x.

Secondly, from the previous sections, it can be seen that the quantum mechanical predictions for state (3.1) violate the Bell inequalities based on this hidden variable picture for the case where the simulated noise in measurements is small. (for values of coherent state amplitude $0.96 \lesssim r \lesssim 1.41$) It can also be seen that the Bell inequality is violated while the noise is of a magnitude less than about 0.19ε.

Thirdly, if the Bell inequality is violated by measurements with some uncertainty $\Delta\varepsilon$ in the number of photons detected by a measurement of X, this uncertainty reflects an uncertainty of $\Delta\varepsilon$ photons for the elements of reality described by the hidden variable description of the system.

With these three things in mind, it can be seen that $\Delta\varepsilon$ can be easily increased to a size where this uncertainty is macroscopic simply by varying ε [6], but the Bell inequality is still violated. Since only macroscopic elements of reality can be still distinguished, then the quantum mechanical predictions seem to be incompatible with *macroscopic* local realism for this state. (as defined in section 1.5).

---

[6]This is in fact inevitable in real experiments where ε is always macroscopic.

Conclusion

The quantum mechanical predictions for both states considered (The higher-spin states and the "circular" superposition of coherent states) were found to be incompatible with complete local realism (i.e. microscopic local realism). More importantly, when a macroscopic quantity was defined as one whose physical value is unknown to within some uncertainty which is itself macroscopic[9], the quantum mechanical predictions for the second state were found to be incompatible with *macroscopic* local realism (see chapter 3).

A common view may be that in the macroscopic limit, quantum mechanics must reduce to a "classical" theory. This would imply that quantum mechanics would be compatible with macroscopic local realism. The results of this investigation seem to cast doubt on this view.

In real experiments, the detectors used will always have some inefficiencies associated with them, and it would be useful if calculations taking these inefficiencies into account were done for the states considered here.

More investigation into the question of compatibility of quantum mechanics with macroscopic local realism should be conducted. It would seem that the state in which incompatibility with macroscopic local realism was found, would be very difficult or impossible to create experimentally with current technology. For this reason it would be very useful if an incompatibility between quantum mechanics and macroscopic local realism were shown for a state which could actually be produced in the laboratory, thus allowing experimental testing of the validity of macroscopic local realism. Another direction which should be pursued is to arrive at a consensus on a definition of "macroscopic".

Appendix A

Additional Proofs on the Higher Spin States

This appendix gives the derivation of the probability distribution of the n, m measurements on the Higher spin states (2.9)(2.8), and its properties (2.13), and the method of determining that the marginal probabilities of measuring n are constant.

A.1 The Probability Distribution

We wish to determine the probability of measuring n bosons at detector A, by measuring the operator $\hat{c}_+^\dagger \hat{c}_+$, and m bosons at detector B, by measuring the operator $\hat{d}_+^\dagger \hat{d}_+$. This is given by equation (2.8) as

$$P_{nm}(\theta, \phi) = \left| \langle n|_{c_+} \langle N - n|_{c_-} \langle m|_{d_+} \langle N - m|_{d_-} |\psi\rangle \right|^2 = \Psi_{nm}^*(\theta, \phi)\Psi_{nm}(\theta, \phi)$$

here $|\psi\rangle$ can be written (in most general form) as (equation (2.6))

$$|\psi\rangle = \frac{\left[\left(\hat{c}_+^\dagger \hat{d}_+^\dagger + \hat{d}_-^\dagger \hat{c}_-^\dagger \right) \cos(\theta - \phi) + \left(\hat{c}_+^\dagger \hat{d}_-^\dagger - \hat{c}_-^\dagger \hat{d}_+^\dagger \right) \sin(\theta - \phi) \right]^N}{N!\sqrt{N+1}} |0\rangle_{c_+} |0\rangle_{c_-} |0\rangle_{d_+} |0\rangle_{d_-}$$

as mentioned before, this depends only on $\chi = \theta - \phi$. The state can be rewritten by expanding via binomial series

$$|\psi\rangle = \frac{1}{N!\sqrt{N+1}} \sum_{r=0}^{N} \binom{N}{r} [\cos(\chi)]^r [\sin(\chi)]^{N-r} \sum_{i=0}^{r} \binom{r}{i} \left(\hat{c}_+^\dagger \hat{d}_+^\dagger\right)^i \left(\hat{c}_-^\dagger \hat{d}_-^\dagger\right)^{r-i} \cdots$$

$$\cdots \sum_{j=0}^{N-r} \binom{N-r}{j} \left(\hat{c}_+^\dagger \hat{d}_-^\dagger\right)^j \left(\hat{c}_-^\dagger \hat{d}_+^\dagger\right)^{N-r-j} (-1)^{N-r-j} |0\rangle_{c_+} |0\rangle_{c_-} |0\rangle_{d_+} |0\rangle_{d_-} \quad \text{(A.1)}$$

$$|\psi\rangle = \frac{1}{\sqrt{N+1}} \sum_{r=0}^{N} \sum_{i=0}^{r} \sum_{j=0}^{N-r} \frac{\sqrt{(i+j)!(N-j-i)!(N-r-j+i)!(r-i+j)!}}{j!i!(r-i)!(N-r-j)!} \cdots$$

$$\cdots [\cos(\chi)]^r [\sin(\chi)]^{N-r} (-1)^{N-r-j} |i+j\rangle_{c_+} |N-j-i\rangle_{c_-} |N-r-j+i\rangle_{d_+} |r-i+j\rangle_{d_-} \quad \text{(A.2)}$$

now, since number states are orthogonal,

$$\langle n| \, p \rangle = \delta_{np} = \delta(n,p) \quad \text{(A.3)}$$

we get

$$\Psi_{nm}(\chi) = \frac{1}{\sqrt{N+1}} \sum_{r=0}^{N} \sum_{i=0}^{r} \sum_{j=0}^{N-r} \frac{\sqrt{(i+j)!(N-j-i)!(N-r-j+i)!(r-i+j)!}}{j!i!(r-i)!(N-r-j)!} \cdots$$

$$\cdots [\cos(\chi)]^r [\sin(\chi)]^{N-r} (-1)^{N-r-j} \delta(n,i+j) \delta(m, N-r-j+i) \quad \text{(A.4)}$$

now one can make the substitution

$$i \to \tfrac{1}{2}(n+m-N+r) \qquad\qquad j \to \tfrac{1}{2}(n-m-r+N) \quad \text{(A.5)}$$

where we require

$$0 \leq i \leq r \qquad\qquad 0 \leq j \leq N-r$$
$$\text{(A.6)}$$
$$i, j \quad \text{are integers}$$

so that we reduce the sum over three variables r, i, j to a sum over just one (r), and in fact some terms in r may drop out also, due to condition (A.6). the conditions (A.6) are required so that the i, j which we are substituting for are actually valid indices for the sums that are being removed by the delta functions.

(A.4) becomes

$$\Psi_{nm}(\chi) = \sqrt{\frac{n!(N-n)!(m)!(N-m)!}{N+1}} \sum_{r \in \mathcal{A}} [\cos(\chi)]^r [\sin(\chi)]^{N-r} (-1)^{\frac{1}{2}(N-r+m-n)} \cdots$$

$$\cdots \frac{1}{[\frac{1}{2}(n+m-N+r)]![\frac{1}{2}(n-m-r+N)]![\frac{1}{2}(r+N-n-m)]![\frac{1}{2}(N-r+m-n)]!} \quad (A.7)$$

where $\mathcal{A}$ is some range of values to be determined. The index r must satisfy the inequalities (A.6), otherwise, the term belonging to r is set to zero by the delta functions in (A.4). (A.6) is eqaivalent to r satisfying *all* of

$$r \le N + n - m \qquad\qquad\qquad r \ge n + m - N$$
$$\qquad\qquad\qquad\qquad\qquad\qquad\qquad\qquad\qquad (A.8)$$
$$r \le N + m - n \qquad\qquad\qquad r \ge N - m - m$$

or in conscise form

$$r \in \mathcal{A} \qquad \equiv \qquad |n + m + N| \quad \le \quad r \quad \le \quad N - |n - m| \qquad\qquad (A.9)$$

also, the requirement that i, j be integers, means that from (A.5), r has the same parity as $n+m+N$. Since $n+m+N$ is constant for any paticular $P_{nm}(\chi)$, only every second r-value in the range given by (A.9) is going to give non-zero terms. thus r can be replaced by $2s$, and so, finally, it can be written

$$\Psi_{nm}(\chi) = \sqrt{\frac{n!(N-n)!(m)!(N-m)!}{N+1}} \sum_{s=\frac{1}{2}|n+m-N|}^{\frac{1}{2}(N-|n-m|)} [\cos(\chi)]^{2s} [\sin(\chi)]^{N-2s} (-1)^{\frac{1}{2}(N+m-n)-s} \cdots$$

$$\cdots \frac{1}{[\frac{1}{2}(n+m-N)+s]![\frac{1}{2}(n-m+N)-s]![\frac{1}{2}(N-n-m)+s]![\frac{1}{2}(N+m-n)-s]!} \quad (A.10)$$

and of course,

$$P_{nm}(\chi) = |\Psi_{nm}(\chi)|^2 \qquad\qquad\qquad\qquad (A.11)$$

which is equivalent to (2.9) and (2.10).

A.2   Properties of the Probability Distribution

In this section, some properties of the probability distribution, given in (2.13) are derived.

Firstly, from (A.10)

$$P_{nm}(\chi + \pi) = \left| \cdots \sum [\cos(\chi + \pi)]^{2s} [\sin(\chi + \pi)]^{N-2s} \cdots \right|^2$$

$$= \left| \cdots \sum [-\cos(\chi)]^{2s} [-\sin(\chi)]^{N-2s} \cdots \right|^2$$

$$= \left| \cdots (-1)^N \sum [\cos(\chi)]^{2s} [\sin(\chi)]^{N-2s} \cdots \right|^2$$

$$= \left| \cdots \sum [\cos(\chi)]^{2s} [\sin(\chi)]^{N-2s} \cdots \right|^2$$

$$P_{nm}(\chi + \pi) = P_{nm}(\chi) \tag{A.12}$$

Also,

$$P_{nm}(\pi - \chi) = \left| \cdots \sum [\cos(\pi - \chi)]^{2s} [\sin(\pi - \chi)]^{N-2s} \cdots \right|^2$$

$$= \left| \cdots \sum [-\cos(\chi)]^{2s} [\sin(\chi)]^{N-2s} \cdots \right|^2$$

$$= \left| \cdots \sum (-1)^{2s} [\cos(\chi)]^{2s} [\sin(\chi)]^{N-2s} \cdots \right|^2$$

$$= \left| \cdots \sum [\cos(\chi)]^{2s} [\sin(\chi)]^{N-2s} \cdots \right|^2$$

$$P_{nm}(\pi - \chi) = P_{nm}(\chi) \tag{A.13}$$

so now if we let $\mu = \frac{\pi}{2} - \chi$, then by (A.13)

$$P_{nm}(\tfrac{\pi}{2} + \mu) = P_{nm}(\tfrac{\pi}{2} - \mu) \tag{A.14}$$

and it can also be easily seen by using (A.12) on (A.13) that

$$P_{nm}(\chi) = P_{nm}(|\chi|) \tag{A.15}$$

If the indices n and m are switched, it can be seen from inspection of (A.10) that

$$P_{mn}(\chi) = P_{nm}(\chi) \tag{A.16}$$

Also, it can be seen from (A.10) that

$$P_{N-n,N-m}(\chi) =$$

$$\left| \cdots \sum_{s=\frac{1}{2}|N-n+N-m-N|}^{N-|N-n-N+m|} \frac{\cdots (-1)^{\frac{1}{2}(N+N-m-N+n)-s}}{[\frac{1}{2}(N-n+N-m-N)+s]! [\frac{1}{2}(N-n-N+m+N)-s]! [\frac{1}{2}(N-N+n-N+m)+s]! [\frac{1}{2}(N+N-m-N+n)-s]!} \right|^2$$

$$= \left| \cdots \sum_{s=\frac{1}{2}|N-n-m|}^{N-|m-n|} \frac{\cdots(-1)^{\frac{1}{2}(N-m+n)-s}}{[\frac{1}{2}(N-n-m)+s]![\frac{1}{2}(N-n+m)-s]![\frac{1}{2}(n+m-N)+s]![\frac{1}{2}(N-m+n)-s]!} \right|^2$$

$$= \left| \cdots \sum_{s=\frac{1}{2}|N-n-m|}^{N-|m-n|} \frac{\cdots(-1)^{\frac{1}{2}(N-m+n)-s}}{[\frac{1}{2}(N-n-m)+s]![\frac{1}{2}(N-n+m)-s]![\frac{1}{2}(n+m-N)+s]![\frac{1}{2}(N-m+n)-s]!} \right|^2$$

$$= \left| \cdots \sum_{s=\frac{1}{2}|n+m-N|}^{N-|n-m|} \frac{\cdots(-1)^{\frac{1}{2}(N-n+m)-s}}{[\frac{1}{2}(N-n-m)+s]![\frac{1}{2}(N-n+m)-s]![\frac{1}{2}(n+m-N)+s]![\frac{1}{2}(N-m+n)-s]!} \right|^2$$

$$P_{N-n,N-m}(\chi) = P_{nm}(\chi) \tag{A.17}$$

And, finally

$$P_{N-n,m}\left(\chi - \tfrac{\pi}{2}\right) =$$

$$\left| \cdots \sum_{s=\frac{1}{2}|N-n+m-N|}^{\frac{1}{2}(N-|N-n-m|)} \frac{[\cos(\chi-\frac{\pi}{2})]^{2s}[\sin(\chi-\frac{\pi}{2})]^{N-2s}(-1)^{\frac{1}{2}(m-N-n+N)-s}}{[\frac{1}{2}(N-N+n-m)+s]![\frac{1}{2}(N-N+n+m)-s]![\frac{1}{2}(N-n+m-N)+s]![\frac{1}{2}(N-m+N-n)-s]!} \right|^2$$

$$= \left| \cdots \sum_{s=\frac{1}{2}|n-m|}^{\frac{1}{2}(N-|m+n-N|)} \frac{[-\sin(\chi)]^{2s}[\cos(\chi)]^{N-2s}(-1)^{\frac{1}{2}(m-n)-s}}{[\frac{1}{2}(n-m)+s]![\frac{1}{2}(n+m)-s]![\frac{1}{2}(m-n)+s]![\frac{1}{2}(2N-m-n)-s]!} \right|^2$$

now let $s = \frac{N}{2} - t$ therefore $t = \frac{N}{2} - s$

$$= \left| \cdots \sum_{t=\frac{1}{2}|m+n-N|}^{\frac{1}{2}(N-|n-m|)} \frac{[\cos(\chi)]^{2t}[\sin(\chi)]^{N-2t}(-1)^{\frac{1}{2}(m-n+N)-t}}{[\frac{1}{2}(N-n-m)+t]![\frac{1}{2}(N-n+m)-t]![\frac{1}{2}(n+m-N)+t]![\frac{1}{2}(N-m+n)-t]!} \right|^2$$

$$P_{N-n,m}\left(\chi - \tfrac{\pi}{2}\right) = P_{nm}(\chi) \tag{A.18}$$

thus the properties (2.13) are proven

A.3 Properties of the Marginal Probabilities

At the beginning of section 2.4, mention is made of the fact that when the marginal probabilities $P_n(\theta), P_m(\phi)$ are evaluated numerically, they are found to be independent of their parameters θ and ϕ respectively. It can also be shown that

$$P_{nm}(0) = \begin{cases} \dfrac{1}{N+1} & \text{if } n = m \\ 0 & \text{otherwise} \end{cases} \tag{A.19}$$

Proof:

when $\chi = 0$, the state is given by equation (2.7) to be

$$|\psi\rangle = \frac{1}{N!\sqrt{N+1}} \left[\hat{c}_+^\dagger \hat{d}_+^\dagger + \hat{c}_-^\dagger \hat{d}_-^\dagger\right]^N |0\rangle_A |0\rangle_B$$

which can be written

$$|\psi\rangle = \sum_{r=0}^{N} \frac{|r\rangle_{c_+} |N-r\rangle_{c_-} |r\rangle_{d_+} |N-r\rangle_{d_-}}{\sqrt{N+1}} \tag{A.20}$$

so by equation (2.8),

$$P_{nm}(0) = \left|\sum_{r=0}^{N} \frac{\delta(n,r)\delta(N-n,N-r)\delta(m,r)\delta(N-m,N-r)}{\sqrt{N+1}}\right|^2$$

$$P_{nm}(0) = \frac{\delta(n,m)}{N+1} \tag{A.21}$$

so the marginal probabilities are

$$P_n(\theta)|_{\chi=0} = \sum_{m=0}^{N} P_{nm}(0) = \sum_{m=0}^{N} \frac{\delta(n,m)}{N+1} = \frac{1}{N+1} \tag{A.22}$$

and because it has been found that $P_n(\theta)$ is independent of θ then the equation (A.22) above holds

for all θ.

Appendix B

Proofs for the "Circular"

Superposition of Coherent States

This appendix gives the derivation of the x-y representation (3.7) of the state (3.1), and the derivation of the theorem used in section 3.3.2 to find the optimum χ, η, ζ parameter range for Bell inequality violations.

B.1   The x-y Representation

Following the discussion in sections 3.1 and 3.2, The state (3.1) is given by

$$|\psi\rangle = \mathcal{N} \int_0^{2\pi} \left| re^{i\mu} \right\rangle_A \left| re^{-i\mu} \right\rangle_B \, d\mu$$

where the normalising factor $\mathcal{N}$ is given by

$$\mathcal{N} = \frac{e^{r^2}}{2\sqrt{\pi \int_0^\pi \exp\left[2r^2 \cos(\omega)\right] \, d\omega}} \tag{B.1}$$

The x-y representation is given by

$$\Psi_{xy}(\theta, \phi) = \langle x|_A \langle y|_B |\psi\rangle \tag{B.2}$$

where $|x\rangle_A$ is the eigenstate with corresponding eigenvalue x of the operator $\hat{x}$ on the light field in region A. The operators $\hat{x}, \hat{y}$ are defined as in (3.3):

$$\hat{x}(\theta) = \tfrac{1}{\sqrt{2}}\left[e^{i\theta}\hat{a} + e^{-i\theta}\hat{a}^\dagger\right] \qquad\qquad \hat{y}(\phi) = \tfrac{1}{\sqrt{2}}\left[e^{-i\phi}\hat{b} + e^{i\phi}\hat{b}^\dagger\right]$$

To obtain Ψ_{xy} we need the expression (3.5)[35].

$$\langle x|\,\alpha\rangle = \pi^{-\frac{1}{4}}\exp\left[-\frac{x^2}{2} - \frac{|\alpha|^2}{2} + \sqrt{2}x\alpha e^{i\theta} - \frac{\alpha^2 e^{2i\theta}}{2}\right]$$

Thus now using (3.1), (B.2) and (3.5) one obtains

$$\Psi_{xy}(\theta,\phi) = \frac{\mathcal{N}}{\sqrt{\pi}}\int_0^{2\pi} d\mu \cdots$$

$$\cdots\exp\left[-\frac{x^2}{2} - \frac{r^2}{2} + \sqrt{2}xre^{i(\mu+\theta)} - \frac{r^2}{2}e^{2i(\mu+\theta)} - \frac{y^2}{2} - \frac{r^2}{2} + \sqrt{2}yre^{-i(\mu+\phi)} - \frac{r^2}{2}e^{-2i(\mu+\phi)}\right] \quad \text{(B.3)}$$

$$\Psi_{xy}(\theta,\phi) = \frac{\mathcal{N}}{\sqrt{\pi}}\exp\left[\frac{x^2}{2} + \frac{y^2}{2} - r^2\right]\cdots$$

$$\cdots\int_0^{2\pi} d\mu\exp\left[-\left(\tfrac{r}{\sqrt{2}}e^{i(\theta+\mu)} - x\right)^2 - \left(\tfrac{r}{\sqrt{2}}e^{-i(\phi+\mu)} - y\right)^2\right] \quad \text{(B.4)}$$

Now make the substitution

$$\theta + \mu = \lambda \qquad \text{and} \qquad \theta - \phi = \chi$$

$$\text{therefore} \quad d\mu = d\lambda \qquad \text{and} \qquad -(\phi+\mu) = \chi - \lambda \tag{B.5}$$

to get

$$\Psi_{xy}(\chi) = \frac{\mathcal{N}}{\sqrt{\pi}}\exp\left[\frac{x^2+y^2}{2} - r^2\right]\int_0^{2\pi}\exp\left[-\left(\tfrac{r}{\sqrt{2}}e^{i\lambda} - x\right)^2 - \left(\tfrac{r}{\sqrt{2}}e^{i\chi}e^{-i\lambda} - y\right)^2\right]d\lambda \quad \text{(B.6)}$$
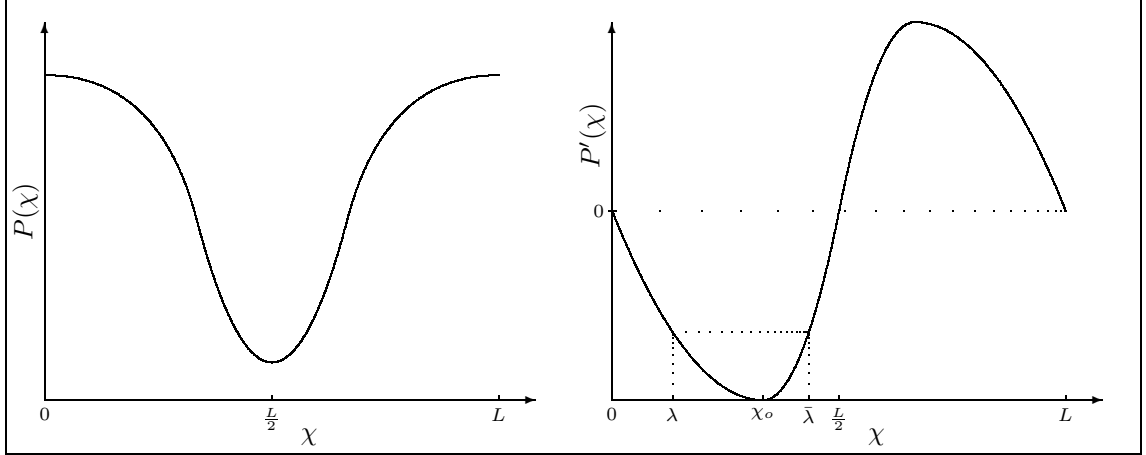
which is equivalent to (3.7), our aim.

B.2   Proof of Equations (3.15)-(3.21)

Initially, we assume we have some function $P(\chi)$ dependent on χ. Now define

$$P'(\chi) = \frac{\partial P(\chi)}{\partial\chi} \qquad \text{and} \qquad B(\chi,\eta,\zeta) = P(\chi) + P(\eta) + P(\zeta) + P(\chi+\eta-\zeta) \tag{B.7}$$

The function $P(\chi)$ is assumed to obey the conditions (3.15)- (3.18), i.e.

Figure B.1: Schematic diagram of the properties of the function $P(\chi)$ used in section B.2

1. $P(\chi + L) = P(\chi)$

2. $P(\chi)$ has maxima at $\chi = 0, L$ and a minimum at $\chi = \frac{L}{2}$ and no other extrema on the interval $\chi \in [0, L]$.

3. $P(L - \chi) = P(\chi)$

4. $P'(\chi)$ has maxima at $\chi = 0, \frac{L}{2}$, a minimum in between at $\chi = \chi_o$, and no other extrema on the interval $\chi \in [0, \frac{L}{2}]$.

It can be immediately seen that due to condition 3,

$$P'(L - \chi) = -P'(\chi) \tag{B.8}$$

Also define $\bar{\chi}$ by

$$P'(\chi) = P'(\bar{\chi}) \qquad \text{and} \qquad \bar{\chi} \neq \chi \tag{B.9}$$

It can be seen that due to condition 4 and (B.8), $\bar{\chi}$ can take on at most one value, and is undefined for $\chi = \chi_o$ and for $\chi = L - \chi_o$ (by (B.8)). Furthermore define the χ values

$$\bar{0} = \frac{L}{2} \qquad \text{and} \qquad \left(\frac{\bar{L}}{2}\right) = 0 \tag{B.10}$$

This situation is represented schematically in figure B.1.

B has some symmetry properties, which can be easily shown using conditions 1 & 3

$$B(L - \chi, \eta, \zeta) = B(\chi, \zeta, \eta) = B(\eta, L - \zeta, \chi) \tag{B.11}$$

These conditions imply that over the parameter range $0 \leq \chi, \eta, \zeta \leq L$ B is duplicated. It turns out that B exhibits unique behaviour only over the range

$$0 \leq \chi, \eta \leq \tfrac{L}{2} \qquad \text{and} \qquad 0 \leq \zeta < L \tag{B.12}$$

and this is the whole range that will be considered, as any extrema outside this range will have the same magnitude as one or more within (B.12). The range (B.12) also implies that $\bar{\chi}, \bar{\eta}, \bar{\zeta}$ will satisfy

$$0 \leq \bar{\chi}, \bar{\eta} \leq \tfrac{L}{2} \qquad \text{and} \qquad 0 < \bar{\zeta} < L \tag{B.13}$$

Now we wish to find the extrema of B. B will have extrema when

$$\frac{\partial B}{\partial \chi} = \frac{\partial B}{\partial \eta} = \frac{\partial B}{\partial \zeta} \tag{B.14}$$

i.e.

$$P'(\chi + \eta - \zeta) = P'(\chi) = P'(\eta) = -P'(\zeta) \tag{B.15}$$

Given the ranges (B.12) above, $\chi + \eta - \zeta$ can be in the range $(-L, L)$. Thus it can be seen (just look at figure B.1) that $P'(\chi + \eta - \zeta = \alpha) = \pm P'(\beta)$ for some β implies that

$$P'(\alpha) = \pm P'(\beta) \quad \Rightarrow \quad \text{one of} \begin{cases} \alpha = \pm\beta \\ \alpha = \pm\bar{\beta} \\ \alpha = \pm(\beta - L) \\ \alpha = \pm(\bar{\beta} - L) \end{cases} \tag{B.16}$$

So combining (B.15) with (B.16) we conclude that extrema of B will occur when

$$\chi + \eta - \zeta = \text{ one of} \begin{cases} \chi \\ \bar{\chi} \\ \chi - L \\ \bar{\chi} - L \end{cases} \text{AND} \chi + \eta - \zeta = \text{ one of} \begin{cases} \eta \\ \bar{\eta} \\ \eta - L \\ \bar{\eta} - L \end{cases} \text{AND} \chi + \eta - \zeta = \text{ one of} \begin{cases} -\zeta \\ -\bar{\zeta} \\ L - \zeta \\ L - \bar{\zeta} \end{cases}$$
$$\tag{B.17}$$

The cases $\chi + \eta - \zeta = \chi - L$ or $\eta - L$ are impossible for χ, η satisfying (B.12). thus (B.17) can be simplified via (B.12)&(B.13) to

$$\text{one of } \begin{cases} \zeta = \eta \\ \chi + \eta - \zeta = \bar{\chi} \\ \chi + \eta - \zeta = \bar{\chi} - L \end{cases} \text{AND one of } \begin{cases} \chi = \zeta \\ \chi + \eta - \zeta = \bar{\eta} \\ \chi + \eta - \zeta = \bar{\eta} - L \end{cases} \text{AND one of } \begin{cases} \chi = \eta = 0 \\ \chi + \eta = \zeta - \bar{\zeta} \\ \chi = \eta = \frac{L}{2} \\ \chi + \eta = L - \zeta - \bar{\zeta} \end{cases}$$
(B.18)

This gives 36 possibilities. By utilising the fact that the variables lie in the ranges (B.12),(B.13), all but 9 of these can be eliminated from consideration. Firstly, extrema may be found at the points shown in figure B.2

Figure B.2: Extrema of $B(\chi, eta, \zeta)$ at boundaries of χ, η, ζ ranges. (see text)

	χ	η	ζ		χ	η	ζ
1)	0	0	0	5)	0	0	$\frac{L}{2}$
2)	$\frac{L}{2}$	$\frac{L}{2}$	$\frac{L}{2}$	6)	0	$\frac{L}{2}$	0
3)	$\frac{L}{2}$	0	$\frac{L}{2}$	7)	$\frac{L}{2}$	0	0
4)	0	$\frac{L}{2}$	$\frac{L}{2}$				

Extrema 1) and 5) give $B = 2P(0)$, while the other five extrema above give $B = 2P(\frac{L}{2})$, which are smaller than $2P(0)$ by condition 2.

The other two possibilities are that extrema are found at parameters given by

$$\chi = \eta, \qquad \bar{\zeta} = L - \bar{\chi}, \qquad \zeta = 2\chi + \begin{cases} \bar{\zeta} \text{ or} \\ -\bar{\chi} \end{cases}$$
(B.19)

Now, because $\bar{\chi} < \frac{L}{2}$ by (B.13), and $\bar{\zeta} = L - \bar{\chi}$, then $\bar{\zeta} > \frac{L}{2}$, so $\bar{\zeta}$ and ζ are in the range $[\frac{L}{2}, L]$, which will give equivalent results if we subtract L from it, now constraining $\zeta, \bar{\zeta}$ to

$$-\frac{L}{2} \leq \zeta, \bar{\zeta} \leq 0$$
(B.20)

This causes the conditions for extrema (B.19) to become

$$\chi = \eta, \qquad \bar{\zeta} = -\bar{\chi}, \qquad \zeta = 2\chi + \begin{cases} \bar{\zeta} \text{ or} \\ -\bar{\chi} \end{cases}$$
(B.21)

which can be used to deduce that extrema will occur on the line

$$\chi = \eta = -\zeta$$

$$0 \leq \chi, \eta, -\zeta \leq \tfrac{L}{2}$$

(B.22)

This is the result used in section 3.3.2.

If $P'(\chi)$ satisfies the additional symmetry postulate

$$P'(\tfrac{L}{2} - \chi) = P'(\chi)$$

(B.23)

then the exact position of these extrema can be located easily. Looking at the conditions (B.21), they indicate that extrema will be found when

$$\chi = \frac{\bar{\chi}}{3} \quad \text{or} \quad \frac{L}{3} + \frac{\bar{\chi}}{3}$$

(B.24)

The additional postulate (B.23) can be seen to imply (via (B.9)) that

$$\bar{\chi} = \tfrac{L}{2} - \chi \quad \text{and} \quad \chi_o = \tfrac{L}{4}$$

(B.25)

so using this and (B.24) we obtain the desired result that extrema will be found at

$$\chi = \frac{L}{8} \quad \text{or} \quad \frac{3L}{8}$$

(B.26)

$$\mathcal{QED}$$

Acknowledgments

I would first and foremost like to thank Dr. Margaret Reid for the ideas behind this work, and continuous support during the course of the project. I couldn't have done it without you!

I'd also like to thank Prof. P.D. Drummond for initially introducing this topic to me. Thanks also go to all the other IVH students this year, who were always around to be pestered by questions, particularily Justin Cooke, Dominic Berry, Simon Hogg, Fleurette Nieuwenberg and Michael Longfren.

I am grateful to Roy Duncan, Michael Gagen, and Marc Elmoutti, and others who I've undoubtedly forgot to mention for help with the computers, as well as David Harris for lending me a much used reference book.

This research was carried out at the Department of Physics at the University of Queensland.

References

[1] A. Einstein, B. Podolsky, and N. Rosen. *Phys. Rev. 47*, page 777, (1935).

[2] Z. Y. Ou, S. F. Pereira, H. J. Kimble, and K. C. Peng. *Phys. Rev. Lett. 68*, page 3663, (1992).

[3] J. S. Bell. *Physics 1*, pages 195–200, (1965).

[4] A. Aspect, P. Grangier, and G. Roger. *Phys. Rev. Lett. 49*, page 91, (1982).

[5] A. Aspect, J. Dailbard, and G. Roger. *Phys. Rev. Lett. 49*, page 1804, (1982).

[6] Y. H. Shih and C. O. Alley. *Phys. Rev. Lett. 61*, page 2921, (1988).

[7] Z. Y. Ou and L. Mandel. *Phys. Rev. Lett. 61*, page 50, (1988).

[8] J. G. Rarity and P.R. Tapster. *Phys. Rev. Lett. 64*, page 2495, (1990).

[9] M. D. Reid and P. Deuar. submitted for pub. *in Phys. Rev. A*, (1996).

[10] E. Schrödinger. *Naturwissenschaften 23*, page 812, (1935).

[11] A. J. Leggett and A. Garg. *Phys. Rev. Lett. 54*, page 587, (1985).

[12] A. J. Leggett. *Directions in Condensed Matter Physics*. World Scientific, Singapore, (1986).

[13] D. Bohm. *Quantum Theory*. Prentice Hall, Englewood Cliffs, NJ, (1951).

[14] M. D. Reid and L. Krippner. *Phys. Rev. A 47*, page 552, (1992).

[15] J. F. Clauser and A. Shimony. *Rep. Prog. Phys. 41*, page 1881, (1978). and references contained therein.

[16] J. F. Clauser and M. A. Horne. *Phys. Rev. D 10*, pages 526–35, (1974).

[17] M. D. Reid. *Phys. Rev. A 40*, page 913, (1989).

[18] M. D. Reid. *Euro. Phys. Lett. 36*, page 7, (1996).

[19] M. Brune, S. Haroche, J. M. Raimond, L. Davidovich, and N. Zagary. *Phys. Rev. A 45*, page 5193, (1992).

[20] L. Davidovich, M. Brune, J. M. Raimond, and S. Haroche. *Phys. Rev. A 53*, page 1295, (1996).

[21] S. Haroche, (1996). Invited talk presented at IQEC, Sydney.

[22] N. D. Mermin. *Phys. Rev. D 22*, page 356, (1980).

[23] A. Garg and N. D. Mermin. *Phys. Rev. Lett. 49*, page 901, (1982).

[24] A. Garg and N. D. Mermin. *Phys. Rev. D* **27**, page 339, (1983).

[25] P. D. Drummond. *Phys. Rev. Lett.* **50**, page 1407, (1983).

[26] N. D. Mermin. *Phys. Rev. Lett.* **65**, page 1838, (1990).

[27] S. M. Roy and V. Singh. *Phys. Rev. Lett.* **67**, page 2761, (1991).

[28] A. Peres. *Phys. Rev. A* **46**, page 4413, (1992).

[29] M. D. Reid and W. J. Munro. *Phys. Rev. Lett.* **69**, page 997, (1992).

[30] G. S. Agarwal. *Phys. Rev. A* **47**, page 4608, (1993).

[31] W. J. Munro and M. D. Reid. *Phys. Rev. A* **47**, page 4412, (1993).

[32] D. Home and A. S. Majumdar. *Phys. Rev. A* **52**, page 4959, (1995).

[33] J. J. Sakurai. *Modern Quantum Mechanics*. Addison-Wesley, Redwood City, Calif., (1985).

[34] H. P. Yuen and V. W. S. Chan. *Opt. Lett.* **8**, page 177, (1983).

[35] W. H. Louisell. *Quantum Statistical Properties of radiation*, page 108. Wiley, (1990).